Structures 71 (2025) 108058

Contents lists available at ScienceDirect

Structures

journal homepage: www.elsevier.com/locate/structures

Synergistic effects of recycled concrete powder, GGBFS, and basalt fibers on mechanical and durability performance of recycled aggregate concrete

Alaa Taha, Wael Alnahhal *

Department of Civil and Environmental Engineering, Qatar University, Doha, Qatar

ARTICLE INFO

Keywords:
Recycled concrete powder
Slag
Basalt fibers
Mechanical performance
Durability
Recycled aggregate concrete

ABSTRACT

This study investigates the sustainable utilization of construction and demolition waste (CDW), specifically recycled concrete powder (RCP), as a partial substitute for cement in concrete. It evaluates the combined effects of basalt fibers (BF) and ground granulated blast furnace slag (GGBFS) on the mechanical and durability properties of recycled aggregate concrete (RAC) incorporating RCP over different curing durations. The study included aggregate and binder characterization tests, along with examining concrete properties, considering parameters such as aggregate type (100 % natural gabbro aggregates (NGA) and 50 % recycled concrete aggregates (RCA)-50 % NGA), binder composition (unary, binary, and ternary blends), and BF addition (0 % and 0.75 % by volume fraction (V_f)). The mechanical properties of concrete were evaluated through compressive strength and flexural properties. Additionally, physical properties such as water absorption, density, and porosity were examined. Durability properties were also evaluated, including the rapid chloride penetration test (RCPT) and surface electrical resistivity (SER). Scanning electron microscopy (SEM) analysis was performed to examine the microstructure of the tested concrete mixes. Test results indicated that the addition of 0.75 % BF to ternary blended RAC with 15 % RCP, 30 % GGBFS, and 55 % ordinary Portland cement (OPC) effectively offset compressive strength reductions, aligning it with the compressive strength of 100 % OPC-based RAC, both with and without BF. Additionally, this mix exhibited a 10.0 % higher flexural tensile strength, a 21.4 % lower charge passing based on RCPT, and a 97.2 % higher SER when compared to 100 % OPC-based RAC with BF. Moreover, the combined effect of incorporating BF and supplementary cementitious materials (SCMs), RCP and GGBFS, yielded superior enhancements in both strength and durability compared to the individual contributions of BF or SCMs when used alone.

1. Introduction

Despite its versatility and reliable performance in concrete, ordinary Portland cement (OPC) exhibits significant environmental impacts, involving vast raw material consumption and energy use during production, contributing to substantial greenhouse gas emissions [1]. Cement production accounts for approximately 5–8 % of anthropogenic CO_2 emissions [2], and constitutes about 45 % of conventional concrete's total cost [3]. On the other hand, coarse aggregates, making up around 60–70 % of the concrete volume, face a staggering yearly estimated demand of about 48.3 billion tons globally [4]. This ever-increasing demand for coarse aggregate leads to rapid depletion of natural quarries, while many regions also grapple with the scarcity of high-quality aggregates, necessitating transport and importation from remote quarries. Despite its significant sustainability drawbacks, concrete remains the second most widely used material, after water, with an annual consumption of 3 tons per capita [5].

The sustainability challenge in the construction industry lies in

Abbreviations: CDW, Construction and demolition waste; RCP, Recycled concrete powder; BF, Basalt fibers; GGBFS, Ground granulated blast furnace slag; RAC, Recycled aggregate concrete; NGA, Natural gabbro aggregates; RCA, Recycled concrete aggregates; V_f, Volume fraction; RCPT, Rapid chloride penetration test; SER, Surface electrical resistivity; SEM, Scanning electron microscopy; OPC, Ordinary Portland cement; SCM, Supplementary cementitious material; FA, Fly ash; SF, Steel fibers; PVA, Polyvinyl alcohol; PP, Polypropylene; BFRP, Basalt fiber reinforced polymer; XRF, X-ray fluorescence spectrometer; XRD, X-ray diffraction spectroscopy; PSD, Particle size distribution; NA, Natural aggregates; GA, Gabbro aggregates; QPMC, Qatar primary materials company; FRC, Fiber reinforced concrete; SSD, Saturated surface dry; ITZ, Interfacial transition zone; CH, Calcium hydroxide; C-S-H, Calcium silicate hydrate; C-A-H, Calcium aluminate hydrate.

* Corresponding author.
E-mail addresses: at1301775@qu.edu.qa (A. Taha), wael.alnahhal@qu.edu.qa (W. Alnahhal).

https://doi.org/10.1016/j.istruc.2024.108058
Received 16 July 2024; Received in revised form 18 November 2024; Accepted 13 December 2024
Available online 23 December 2024

reducing dependency on natural aggregates and Portland cement in concrete production [6]. Thus, scholars have garnered significant attention towards investigating cost-effective and environmentally friendly alternative construction materials for green concrete. A common practice in waste management involves processing construction and demolition waste (CDW) into recycled concrete aggregates (RCA) to replace natural aggregates in concrete, mitigating environmental hazards. Studies on utilizing RCA as a replacement for natural aggregates have been well established in the literature [7]. Numerous studies have explored the impact of RCA incorporation on concrete workability [8–10], density [11,12], compressive strength [8,9,13,14], flexural strength [15–17], tensile strength [11,15], and elastic modulus [11,18]. Typically, increasing the replacement ratio of RCA in concrete results in reduced compressive strength, flexural tensile strength, and workability [19]. However, some studies have reported insignificant reductions in mechanical properties with up to 50 % RCA replacement [20,21].

Supplementary cementitious materials (SCMs) are powders that can partially replace clinker in cement production or Portland cement in concrete production [22]. Studies have explored SCMs like ground granulated blast furnace slag (GGBFS) and fly ash (FA) [23–27]. However, for FA, the mass production feasibility is doubtful due to limited local sources [22]. The supply chain of FA for concrete production in the U.S. and other countries is threatened, as about 40 % of coal-fired power plants have shut down in recent years. Moreover, the UK and Netherlands also plan to close all coal-fired power plants by 2025 and 2030, respectively [22,28]. Meanwhile, the demand for cement is projected to surpass 6 Gt by 2050 [29].

GGBFS, an industrial by-product of blast furnaces during iron production, forms by extinguishing the molten by-products of steel making with water, resulting in a granular and glassy product that is subsequently dried and ground [30]. It can replace OPC at replacement ratios of 35–70 %[31]. GGBFS's typical glass composition occupies 85 % of its overall volume, with a specific gravity ranging from 2.7 to 2.9 (lower than OPC) and a bulk density of 1200 kg/m^3–1300 kg/m^3 [32]. Regarding the workability of concrete incorporating GGBFS, several studies [24–26] reported improved workability with increasing GGBFS replacement ratio attributed to better dispersion of cementitious particles along with the denser and smoother particle surfaces, compared to OPC, leading to reduced water absorption during mixing [33]. Concerning compressive strength, several studies [34–36] reported a reduction in early strength development with increased GGBFS replacement, yet comparable long-term compressive strength. As for durability, GGBFS inclusion in concrete led to enhanced chloride resistance compared to conventional concrete, as reported by various studies [25,37,38].

Recycled concrete powder (RCP) is a promising alternative to OPC due to its abundance as it is a by-product formed during the production of RCA with particles below 150 μm and constitutes about 20–30 % of the generated CDW by weight. However, its average particle size above 75 μm results in low reactivity as a concrete binder [39]. Thus, using the generated RCP as filling material in construction is more suitable than SCMs applications [6,40]. Other studies produced RCP by crushing and grinding RCA [41,42]. RCP shares a composition similarity with FA, containing high SiO_2 and Al_2O_3 levels, promoting pozzolanic activity [6,43,44]. To utilize RCP as an SCM, further grinding is necessary for proper particle size. Several studies reported that RCP becomes highly reactive after further grinding, making it a viable SCM in concrete production [45–47].

Regarding fresh properties of concrete, concrete workability declines with increased cement replacement by RCP [48]. Generally, higher RCP replacement ratios result in reduced concrete compressive and flexural strengths when RCP's fineness is lower than that of cement. Conversely, higher RCP's fineness improves concrete durability in terms of chloride and water ingress [39]. On the other hand, Xiao et al. [6] observed negligible reductions in mechanical properties of concrete with up to 30 % replacement of OPC by RCP. Furthermore, Horsakulthai [42] examined RCP replacement ratio effects on compressive strength, electrical resistivity, and porosity of self-compacting mortars after 28 days, suggesting that the optimal replacement of OPC by RCP is 20 %, which insignificantly affected the 28-day compressive strength. However, 20 % RCP mortars decreased electrical resistivity by 18.1 % and increased porosity by 6.3 %. Additionally, Duan et al. [49] studied the combined effect of RCA and RCP on self-compacting concrete durability using two RCP replacement ratios (10 % and 20 %) and four RCA replacement ratios (0 %, 25 %, 50 %, and 100 %). It was found that up to 50 % RCA with 10 % RCP showed a minor increase in chloride concentration compared to concrete with no RCA and RCP.

Additionally, researchers have utilized structural fibers to enhance the tensile and flexural strength of recycled aggregate concrete (RAC) by controlling crack propagation. Various fibers, including steel fibers (SF), polyvinyl alcohol (PVA) fibers, polypropylene (PP) fibers, and basalt fibers (BF), have been studied [50–55]. These investigations demonstrated improved splitting tensile strength [50,53] and flexural strength [50]. Some studies reported enhanced compressive strength with structural fibers[53,54], while others found no significant effect [51,52] or even a reduction in compressive strength [55]. Furthermore, previous studies have indicated that the use of BF in concrete improved the bond durability of basalt fiber reinforced polymer (BFRP) bars to concrete [56] and enhanced the shear capacity of BFRP bars reinforced large-scale beams [57]. Concerning the effect of BF on RAC, Zhang et al. [58] investigated basalt fiber-reinforced recycled aggregate concrete (BFRRAC) under triaxial compression. The study reported maximum increases of 352.5 % and 224.6 % in peak and elastic modulus, respectively, with the increase of fiber dosage and confining pressure. Additionally, Zhang et al. [59] observed a maximum of 7.8 % increase in peak load of BFRRAC-filled square steel tubular columns under eccentric compression with increasing fiber dosage, while an insignificant effect was observed under axial compression [60]. In terms of optimum volume fraction of BF, previous studies [61,62] reported that the maximum improvement in terms of concrete mechanical properties was achieved at 0.75–1 % BF volume fraction.

Based on the conducted literature review, few studies have investigated the combined use of RCA and RCP in concrete, and limited research has focused on the durability properties of concrete incorporating RCP. Furthermore, there is a gap in the literature concerning the durability of BF-reinforced green RAC. This article aims to enhance the mechanical and durability properties of green concrete incorporating RCA at 50 % by direct volume replacement of natural aggregates and RCP at 15 % by weight of binder, using GGBFS and BF. Eight concrete mixes were produced in this study, and the replacement ratios were chosen based on previous studies [20,21,63,64] with minimal adverse effects on concrete's mechanical properties. Fresh concrete properties were assessed through the slump test, while concrete physical properties comprised concrete density, absorption, and porosity. Moreover, the mechanical properties of concrete were assessed through compressive strength and flexural tensile strength. Additionally, concrete durability properties were assessed using the rapid chloride penetration test (RCPT) and surface electrical resistivity (SER). Both mechanical and durability properties were evaluated after 28 days and 90 days of curing. The microstructure characterization methods for the powders used included laser diffraction, X-ray fluorescence (XRF), X-ray diffraction (XRD), and scanning electron microscopy (SEM) to determine particle size distribution (PSD), elemental composition, phase identification, and particle shape, respectively. Additionally, SEM was used to investigate the microstructure of the concrete mixes in this study.

GGBFS enhances the durability of concrete, while the utilization of RCP offers environmental benefits. Both GGBFS and RCP are economically feasible due to their lower cost compared to OPC [65,66]. Although the individual effects of RCA, RCP, and BF have been investigated in previous studies, the focus of the current study lies in examining the combined use of these materials in RAC. The novelty of the current study is in examining the synergistic effects of incorporating these materials

together to understand how their interactions influence both the mechanical and durability properties of RAC.

2. Materials and methods

2.1. Materials

2.1.1. Aggregates

In this study, two aggregate variants were employed: natural aggregates (NA) and RCA. The utilized natural aggregates comprised gabbro aggregates (GA), an igneous rock exhibiting a dark-grey color (Fig. 1(a)). In Qatar, GA is predominantly imported, notably from Oman, due to its scarcity, necessitated by the high demand within the construction sector [67]. Conversely, the RCA originated from the recycling facility of Qatar Primary Materials Company (QPMC), entrusted with managing CDW. The distinctive trait of the RCA lay in its markedly porous and rugged surface texture (Fig. 1(b)). The coarse aggregates ranged in size from 5 mm to 10 mm, labeled as 10 mm aggregates, and from 10 mm to 20 mm, designated as 20 mm aggregates. Concrete production involved a weight proportioning ratio of 2:3 for 10 mm aggregates to 20 mm aggregates. Additionally, commercial washed sand constituted the fine aggregates in the concrete blends.

2.1.2. Commercial and recycled powders

A universal OPC CEM I 42.5 R was utilized for all concrete mixes. Additionally, GGBFS was incorporated to enhance concrete durability via ternary designs involving OPC and RCP. RCP was obtained from RCA by crushing, ball milling, and sieving, ensuring that 90 % of the powder passed through a No. 270 sieve (53 μm aperture) by wet sieving. Fig. 2 depicts RCP production steps, sourced from the same RCA utilized for coarse aggregates. The 20 mm RCA was initially crushed using a jaw crusher to reduce sizes under 5 mm, followed by sieving through No. 4 (4.75 mm) sieve. Product underwent 110°C oven drying for 24 h, then ball milling within a 15 L stainless steel jar using stainless steel balls (25 mm to 60 mm, totaling 28 kg) with 7.5 kg of 4.75 mm crushed RCA. After experimentation, ball milling lasted 2.5 h at roughly 75 % of its critical speed. Subsequently, only sub-75 micron powders were collected as RCP, ensuring its fineness exceeded or matched OPC, as per Ma et al. [64].

2.1.3. Basalt fibers

The employed BF had a fiber content of 46 % and were sourced from ReforceTech AS, Ryken, Norway [68]. These fibers were amalgamated with a vinyl ester polymeric resin to yield BF, demonstrated in Fig. 3. Evidently, the fibers exhibited helical windings for enhanced adhesion with the surrounding concrete. BF dimensions were 43 mm in length and 0.72 mm in diameter. The BF had a tensile strength of 900 MPa, a density of 2.1 g/cm^3 , and an aspect ratio of 59, as per the manufacturer's datasheet.

2.1.4. Mix design

In this investigation, a total of eight concrete mixes were prepared. One of the eight concrete mixes comprised 100 % OPC as binder composition and 100 % NGA as aggregate composition. The remaining concrete mixes were made with RAC which included substituting 50 % of NGA with RCA by volume. For binary concrete blends, OPC was either replaced with RCP at 15 % replacement level or with GGBFS at 45 % replacement level, both by weight. In the case of ternary concrete blends, a combination of 15 % RCP and 30 % GGBFS replaced OPC by weight. Moreover, BF were added to green concrete mixes at 0.75 % volume fraction to assess the mechanical and durability of fiber reinforced concrete (FRC). Both NGA and RCA were in a saturated surface dry (SSD) state. SSD was achieved by immersing aggregates for 24 h, then air drying until surface became dry aligning with Alnahhal and Aljidda's recommendation [51]. The specimens' nomenclature followed the following sequence: Concrete type-aggregate type-binder composition, illustrated in Fig. 4. For example, F-R-GRO is an FRC that incorporated RCA at 50 % replacement ratio with a ternary binder blend comprising 30 % GGBFS, 15 % RCP, and 55 % OPC. P-R-O is the control mix used to assess the binder composition effect. All concrete mixes incorporated a 0.5 water-to-binder ratio. Table 1 details the concrete ingredient proportions for all the mixes. Binders were replaced by mass. Superplasticizer was added to maintain a 65 mm ± 10 mm slump. Mixing followed ASTM C192 [69]. For FRC, RCA, NA, and BF were dry-mixed for 1 min, wetted with some of the mixing water, and mixed for an additional 30 s. Other concrete ingredients were added, mixed for 3 min, rested for 3 min, and then finally mixed for an additional 2 min before pouring concrete.

2.2. Methods

2.2.1. Characterization of aggregates

Sieve analyses were conducted on RCA and NGA at a 2:3 proportion ratio for 10 mm to 20 mm aggregates to verify compliance with ASTM C33/C33M −18 [70] gradation limits. Physical properties including specific gravity and water absorption (ASTM C127–15 [71]), abrasion resistance (ASTM C131 [72]), and soundness (ASTM C88[73]) were also assessed.

2.2.2. Characterization of recycled and commercial powders

This investigation assessed powder density (OPC, GGBFS, RCP) following ASTM C188[74]. In this test, Le Chatelier flask along with

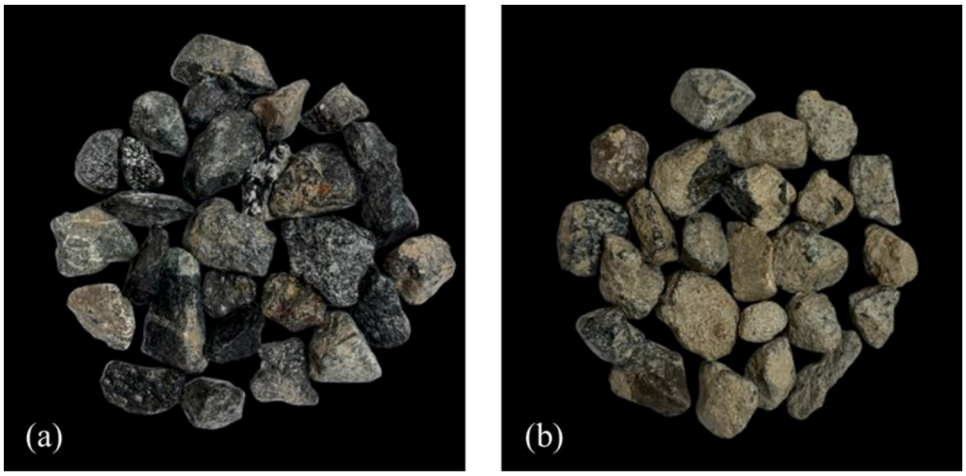

Fig. 1. (a) NGA; (b) RCA.

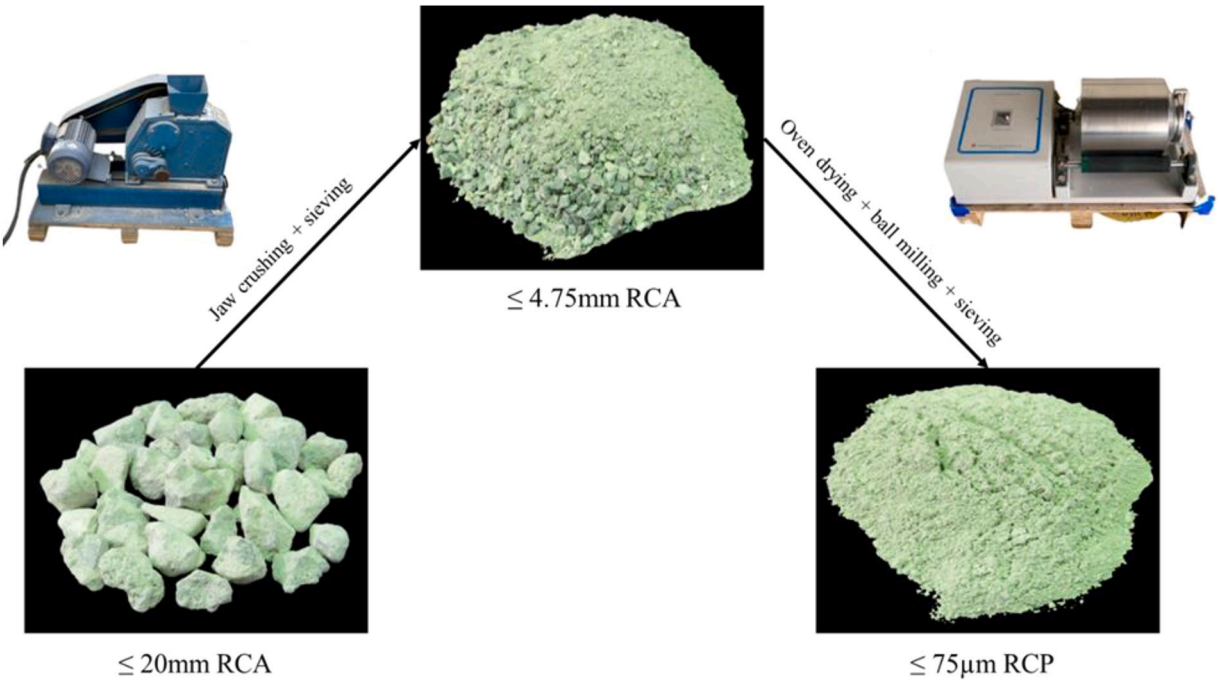

Fig. 2. Production process of RCP.

Fig. 3. BF used in this study.

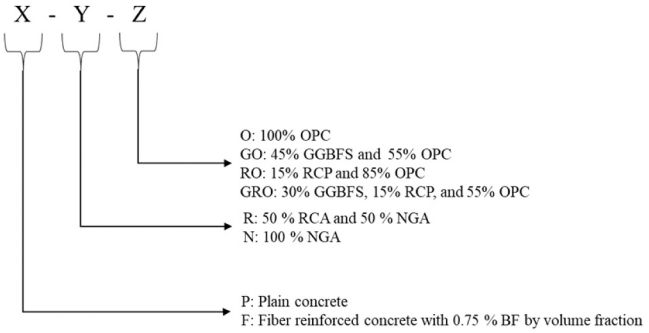

Fig. 4. Illustration for specimen identification.

kerosene with a specific gravity of 0.77 as liquid were used following the standard procedure to measure the density of the used binders. Furthermore, the reactivity of the produced RCP was assessed based on the 7-day compressive strength mortar as per ASTM C618 [75]. According to ASTM C618 [75], an SCM is considered reactive if a mortar with 20 % SCM replacing OPC retains at least 75 % of the compressive strength of a mortar with 100 % OPC after 7 and/or 28 days. Particle morphology and surface texture were observed via SEM, using NOVA NANOSEM 450 for RCP, OPC, and GGBFS. Particle size distribution was analyzed using Malvern Mastersizer3000. Fineness was determined by blain air permeability (ASTM C204–18e1[76]). The chemical composition of powders was analyzed via XRF, and mineralogy via XRD with S2 Puma Bruker®.

2.2.3. *Fresh and mechanical properties of concrete*

Concrete slump test according to ASTM C143/C143M-15a[77] was performed upon mixing completion. Compressive strength was assessed through three identical 100 × 200 mm cylinders as per ASTM C39/C39M-21[78] at 28 and 90 days with 0.2 MPa/sec loading rate. Flexural tensile strength was evaluated on three identical 100 × 100 × 500 mm prisms as per ASTM C1609[79], using a displacement-controlled Instron machine (0.1 mm/min) as shown in Fig. 5.

2.2.4. *Durability tests for concrete*

2.2.4.1. Surface electrical resistivity. SER tests followed AASHTO TP 95–11 [80] via the four-probe (Wenner-Array) technique using GIATEC SurfTM device (Fig. 6). The method gauges resistivity in water-saturated cylindrical concrete specimens measuring 200 mm in length and 100 mm in diameter to promptly evaluate chloride ion penetration resistance and concrete permeability. An AC potential from outer Wenner pins induces current flow in the concrete; while the potential difference is measured between the inner pins. Surface electrical resistivity (kΩ-cm) calculation uses current, potential difference, and the affected zone of the cylindrical sample. Table 2 correlates resistivity with chloride penetration for 100 mm× 200 mm cylindrical samples (Wenner Probe 1.5 cm) as per AASHTO TP 95–11 [80]. Each mix had

Table 1
Concrete mix proportions (kg/m^3).

Mix ID	Cement	GGBFS	RCP	RCA	NGA	Fine aggregates	Water	SP	BF
P-R-O	353.00	-	-	485	548	666	177	1.08	-
P-N-O	353.00	-	-	-	1096	666	177	0.90	-
P-R-GO	194.15	158.85		485	548	666	177	0.99	-
P-R-RO	300.05	-	52.95	485	548	666	177	1.26	-
P-R-GRO	194.15	105.90	52.95	485	548	666	177	1.17	-
F-R-O	353.00	-	-	485	548	666	177	1.26	14.25
F-R-RO	300.05	-	52.95	485	548	666	177	1.45	14.25
F-R-GRO	194.15	105.90	52.95	485	548	666	177	1.35	14.25

Fig. 5. Flexural tensile strength test setup.

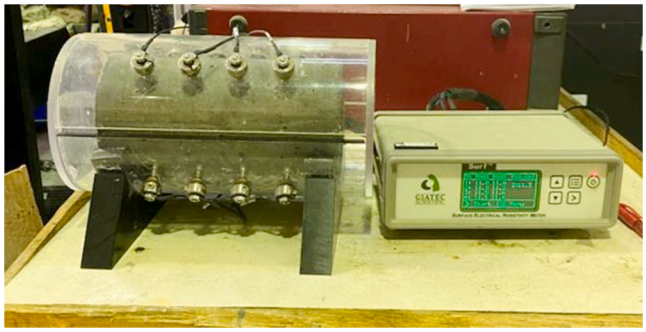

Fig. 6. SER test conducted in this study.

three identical cylindrical samples, tested at 28 and 90 days of curing. The concrete cylinders were towel-dried after removal from curing tank and promptly tested.

Table 2
Chloride ion penetration assessment based on surface electrical resistivity. [80].

Chloride Ion Penetration	Surface Resistivity (kΩ-cm)
High	< 12
Moderate	12–21
Low	21–37
Very Low	37–254
Negligible	> 254

2.2.4.2. Chloride ion penetration. The RCPT was conducted following ASTM C1202 [81], using GIATEC PermaTM apparatus (Fig. 7). Each mix involved two 200 mm × 100 mm cylindrical concrete samples. RCPT specimens were extracted by slicing cylinders parallel to the top into 50 mm thick sections using a water-cooled saw. Samples were air-dried for ≥ 1 h and silicon-coated on sides to ensure unidirectional chloride ingress. After that, specimens underwent 3 h of vacuum desiccation (≤ −28 in Hg) followed by 1-h saturation at the same pressure, specimens rested for 18 h ± 2 h. The test setup involved exposing samples' surfaces to a 3 % mass concentration of Sodium Chloride (NaCl) solution (negative terminal) and 0.3 M Sodium Hydroxide (NaOH) (positive terminal). Maintaining 60 volts dc, current readings were taken at 30-min intervals over 6-h testing. Total charge passed quantified the chloride ion resistance of concrete. RCPT was conducted at 28 and 90 days of curing. Total charge was calculated using the subsequent equation:

$$Q = 900\ (I_0 + 2I_{30} + 2I_{60} + \ldots + 2I_{300} + I_{360}) \quad (1)$$

where Q represents the total charge (coulombs) through the RCPT specimen, I_0 is the initial current (amperes) right after applying constant DC voltage, and I_t is the current (amperes) recorded at time t after voltage application.

2.2.5. Density, absorption, and porosity

The physical properties of concrete, including density, absorption, and porosity, were determined following ASTM C642–21 [82].

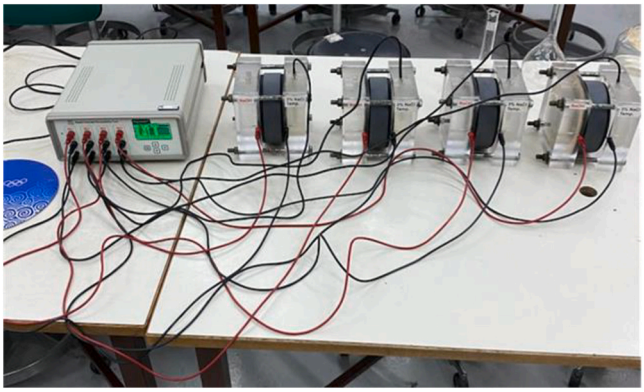

Fig. 7. RCPT instrument used in this study.

Cylindrical concrete slices, 50 mm thick and 100 mm in diameter, were obtained from cylinders using a water-cooled saw. Each sample exceeded the 800 g minimum mass requirement. After oven drying at 110 °C ± 5 °C, mass was monitored every 24 h until differences between successive readings were < 0.5 %. The final reading was denoted as oven-dry mass (A). Post-oven drying, specimens were soaked for ≥ 48 h, and their weights were monitored similarly. After surface water removal, readings continued (<0.5 % difference). Final reading was denoted as saturated mass after immersion (B). Subsequently, specimens were boiled for 5 h, then cooled for more than 14 h. After removing surface moisture, the mass was recorded, marking the saturated mass after boiling (C). The specimen was suspended, and apparent mass was determined (D). With A, B, C, and D established, subsequent calculations determined the following physical properties of concrete.

$$\text{Concrete absorption after water immersion, } \% = \left[\frac{B-A}{A}\right] \times 100 \quad (2)$$

$$\text{Concrete absorption after water immersion and boiling, } \% = \left[\frac{C-A}{A}\right] \times 100 \quad (3)$$

$$\text{Dry concrete bulk density, } \left(\frac{Mg}{m^3}\right) = \left[\frac{A}{C-D}\right] \times \rho = g_1 \quad (4)$$

$$\text{Bulk concrete density after water immersion, } \left(\frac{Mg}{m^3}\right) = \left[\frac{B}{C-D}\right] \times \rho \quad (5)$$

$$\text{Apparentconcretedensity, } \left(\frac{Mg}{m^3}\right) = \left[\frac{A}{A-D}\right] \times \rho = g_2 \quad (6)$$

$$\text{Porosity(Volume of permeable pore space), } \% = \left[\frac{g_2-g_1}{g_2}\right] \times 100 \quad (7)$$

$$\text{Where}\rho \text{ is the water density} = 1\frac{Mg}{m^3} \quad (8)$$

2.2.6. Microstructural analysis

In this investigation, microstructural analysis of both binding powders and concrete was conducted via SEM images following ASTM C1723–16 [83]. SEM images were captured using the NOVA NANOSEM 450 instrument. Binding powders' samples for SEM encompassed OPC, GGBFS, and RCP. Concrete SEM samples were extracted from fractured surfaces post 28-day compressive strength tests.

3. Results and discussion

3.1. Aggregates characterization

The sieve analysis, depicted in Fig. 8, indicated that the selected proportioning ratio of 2:3 (10 mm aggregates to 20 mm aggregates) was in compliance with the upper and lower grading limits of the ASTM C33/C33M −18[70]. Table 3 presents properties of tested RCA and NGA, revealing RCA's water absorption exceeding the QCS-2014 [84] limit.

3.2. Commercial and recycled powders characterization

Table 4 presents the chemical composition of the used powders via XRF analysis and powders densities. RCP exhibited notable SiO_2 prominence. Additionally, Al_2O_3 and CaO appeared as major components. SiO_2 dominance results from silicious sand, aggregate sources, and

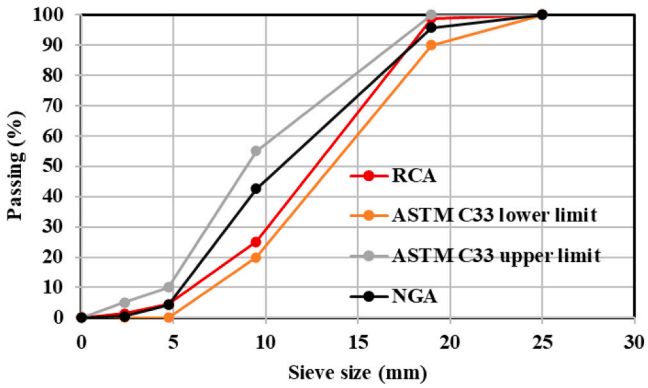

Fig. 8. Sieve analysis based on the combination ratio of coarse aggregates used in this study.

cement hydrates [85]. RCP's lower CaO (28.5 %) versus OPC (73.2 %) is attributed to the adhered mortar surrounding RCA. This potentially contains more silicious components and less cement components, including hydrated cement with calcium silicate hydrate (C-S-H) gels and calcium hydroxide (Ca(OH)2) [42]. Density-wise, RCP displayed 2.70 g/cm^3, less than GGBFS (2.85 g/cm^3) and OPC (3.1 g/cm^3). Furthermore, the produced RCP exhibited a 7-day activity index of 89 % which is significantly higher than the specified minimum threshold value of 75 % for an SCM to be deemed reactive as per ASTM C618 [75].

Fig. 9 illustrates SEM images portraying the particle shapes of the powders used. Observably, binders exhibited angular and irregular particle forms. RCP displayed particles with relatively rougher surface texture and surface micropores, distinct from other powders. GGBFS demonstrated particles with comparably smooth, glassy surfaces. Generally, GGBFS particles are distinguishable by sharp edges, angles, and extended shapes, while OPC particles leaned more toward spherical morphology[86]. It can be observed, from Table 4, that the fineness of RCP was the highest compared to the other used powders, which can be confirmed by the visual illustration of the PSD curves of Fig. 10. Furthermore, Fig. 11(a), Fig. 11(b), and Fig. 11(c) illustrate XRD analyses of the cementitious powders employed in this study. Within the GGBFS pattern, a broad feature appeared between 2θ angles of 22° and 38°, indicating a possible presence of an amorphous or vitreous phase, as consistent with Shi et al.'s findings [87]. This vitreous phase typically forms due to the rapid cooling of molten slag during the quenching process. Unlike amorphous materials, which lack a long-range crystalline structure, both RCP and OPC exhibited well-defined diffraction peaks. In the case of RCP, primary crystalline phases included Plombierite and Quartz low (Silicon Oxide), evident by a sharp peak at a 2θ angle of 26.8°. The dominance of this peak, associated with plombierite, a C-S-H mineral frequently present in concrete powders, implied its formation during the hydration of cementitious material. Concurrently, the presence of quartz at the same peak indicated the occurrence of crystalline silica, a typical aggregate constituent. Notably, the XRD pattern also displayed sharp peaks between 2θ angles of 26° and 30°, corresponding to various minerals including tremolite, calcite, and labradorite. Tremolite, an amphibole mineral, contributes to concrete's mechanical properties, while calcite may result from additives or secondary mineral formation. The detection of labradorite, a plagioclase feldspar, is of significance to the strength and durability of the concrete. Conversely, the XRD of OPC revealed the main components as Hatrurite (tricalcium silicate oxide) or alite, accompanied by calcite, represented by sharpest peaks at a 2θ angle of 32.3°. Similar phases were observed in other OPC studies [88,89]. Generally, Alite contributes to early strength development and mechanical properties, while calcite may influence setting time, workability, and durability.

Table 3
Aggregates' properties.

Type of aggregate	Specific gravity (SSD)	Specific gravity (Dry)	Specific gravity (APP)	Water absorption (%)	Soundness (%)	Abrasion Loss (%)
RCA	2.54	2.39	2.80	6.00	12.60	17.50
NGA	2.87	2.84	2.93	1.07	2.20	8.89

Table 4
Chemical and physical properties of binding powders used for concrete mixes.

Chemical property	RCP	Cement	GGBFS
MgO	10.5 %	0.9 %	4 %
Al_2O3	11.5 %	1.4 %	12.9 %
SiO_2	38 %	15.2 %	28.3 %
SO_3	0.9 %	2.7 %	1 %
K_2O	0.6 %	1.1 %	0.6 %
CaO	28.5 %	73.2 %	50.8 %
TiO_3	0.3 %	0.2 %	0.6 %
Cr_2O_3	0.1 %	0 %	0 %
MnO	0.2 %	0.1 %	0.3 %
Fe_2O_3	9 %	4.2 %	1 %
ZrO_3	0 %	0 %	0.1 %
SrO	0.1 %	0.4 %	0.1 %
Sc_2O_3	0.2 %	0.5 %	0.4 %
Cl	0.1 %	0 %	0 %
%(Si, Al, Fe) oxides	58.5 %	20.8 %	42.2 %
Density (g/cm^3)	2.70	3.10	2.85
Fineness Specific surface area (m^2/kg)	515.99	239.06	327.00
Activity index	89 %	-	-

3.3. Compressive strength of concrete

Fig. 12(a) illustrates the compressive strengths of all concrete mixes over two curing periods, 28 and 90 days. Additionally, Fig. 12(b) demonstrates the influence of aggregate type on concrete compressive strength. Notably, employing 50 % RCA in P-R-O led to a reduction in compressive strength of 8.3 % and 12.3 % after 28 and 90 days of curing, respectively, compared to P-N-O containing 100 % NGA. This strength decrease is attributed to the inferior interfacial transition zone (ITZ) properties of RCA, influenced by aged and adhered mortar. The high water absorption of RCA from residual mortar contributed to water uptake during mixing, potentially impairing cement hydration [90]. Moreover, RCA's bonding to the cementitious matrix is weaker than that of NGA, thereby reducing compressive strength, which hinges greatly on aggregate-matrix bonding [91,92]. Furthermore, as shown in Fig. 12(c), the rate of compressive strength increase from 28 to 90 days in P-R-O was comparatively slower than in P-N-O. This behavior is attributed to NGA's ITZ densification during curing, surpassing that of RCA's ITZ. Comparable findings were reported by Fallahnejad et al.[90].

Examining binder composition influence in Fig. 12(a) reveals that, with 45 % GGBFS replacing OPC in P-R-GO, 93.3 % of P-R-O's strength was maintained. This slight reduction can be attributed to GGBFS's slower hydration rate due to its lower chemical reactivity compared to OPC[93]. Introducing 15 % RCP as a partial replacement to OPC in P-R-RO yielded comparable, slightly elevated compressive strength compared to 100 % OPC concrete (P-R-O). This enhancement might arise from RCP's finer nature, boosting pozzolanic activity and pore filling within RCA, sustaining overall RAC performance. A similar outcome was reported by Ma et al. [64] when employing a 15 % concrete waste powder replacement. Furthermore, the ternary blend of 15 % RCP, 30 % GGBFS, and 55 % OPC in P-R-GRO retained 84.4 % and 74.4 % of P-R-O's 28- and 90-day compressive strengths, respectively. This notable decrease can be attributed to lower CaO content in the binder composition, as both RCP and GGBFS exhibited less CaO than OPC.

Fig. 12(d) illustrates the influence of incorporating 0.75 % BF into the concrete mixture. Notably, the addition of BF exhibited negligible impact on the compressive strength of concrete blends containing OPC and RCP, as seen in cases like F-R-O and F-R-RO. However, when introducing 0.75 % BF to the RAC mixture with ternary binders, exemplified by F-R-GRO, substantial enhancements of 17.8 % and 25.2 % were observed in compressive strengths at 28 and 90 days, respectively, compared to P-R-GRO. Remarkably, the inclusion of 0.75 % BF counteracted the compressive strength reduction observed in P-R-GRO compared to the control mix of this study. The augmentation of compressive strength due to the incorporation of structural fibers into GGBFS and RCP-containing concrete can be attributed to improved bond strength between the structural fibers and the surrounding concrete matrix. This enhancement stems from the presence of SCMs in the concrete, leading to a refined interface between the binder matrix and fibers [94]. Furthermore, the positive net gain in compressive strength within F-R-GRO can be attributed to the role of SCMs in fostering additional C-S-H formation and enhancing the ITZ around the fibers. The increased bond strength between fibers and the surrounding binder matrix owes itself to the heightened micro-hardness of the ITZ, further facilitated by the presence of SCMs [95,96].

3.4. Flexural tensile properties of concrete

Fig. 13 illustrates images capturing flexural failure in the tested specimens. The plain concrete samples exhibited a brittle failure mode, characterized by crack initiation at nearly zero deflection. Consequently, these specimens displayed no residual flexural strength or toughness, but rather displayed a complete fracture across the entire section depth upon failure. In contrast, the majority of specimens reinforced with BF did not fracture into two distinct parts after failure. This can be attributed to the bridging effect of BF, contributing to an enhancement in the tension stiffening of the concrete. The incorporation of BF led to improved crack resistance and increased the concrete's capacity to withstand tension forces.

Fig. 14 depicts the flexural tensile strength of all concrete mixes at two curing periods, 28 and 90 days. Clearly, prolonging the curing duration had a positive effect on the flexural tensile strength. However, the rate of increase in flexural tensile strength is comparably lower than that observed for compressive strength. In plain concrete samples, the enhancement in flexural tensile strength after 90 days of curing ranged from 6.2 % to 15.0 % compared to the corresponding strength at 28 days. This implies that the flexural tensile strength continues to improve with prolonged curing, albeit at a reduced pace compared to the rate of compressive strength improvement. Conversely, for FRC specimens, the rate of increase in flexural tensile strength after 90 days of curing varied from 2.0 % to 19.6 % compared to the strength at 28 days. Moreover, the type of aggregate significantly influenced the flexural tensile strength of concrete. The experimental findings elucidate that introducing 50 % RCA into concrete (P-R-O) led to an 11.9 % decrease in flexural tensile strength when compared to concrete containing 100 % NGA (P-N-O) after 28 days of curing. This reduction can be attributed to the comparatively lower elastic modulus of RCA in contrast to NGA [97].

The type of binder composition also plays a crucial role in influencing the flexural tensile strength of RAC. Notably, both the P-R-O and P-R-RO concrete mixes exhibited comparable and heightened flexural tensile strengths when compared to the other binder combinations investigated in this study. This trend can be attributed to their higher compressive strengths relative to the other mixes. The P-R-O and P-R-RO blends notably showcased the highest 28-day flexural tensile strengths,

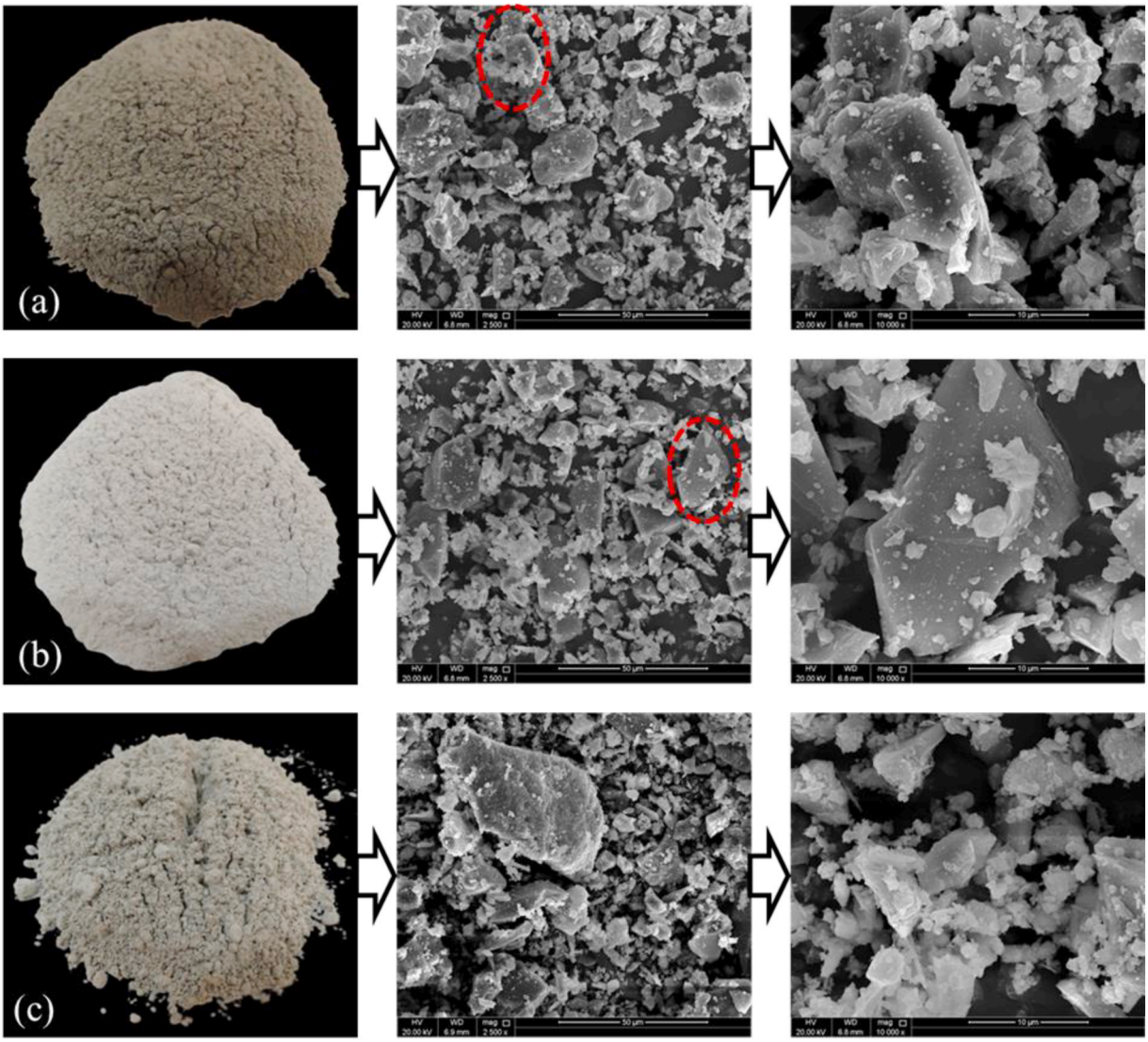

Fig. 9. Photos and SEM images of: (a) OPC; (b) GGBFS; and (c) RCP.

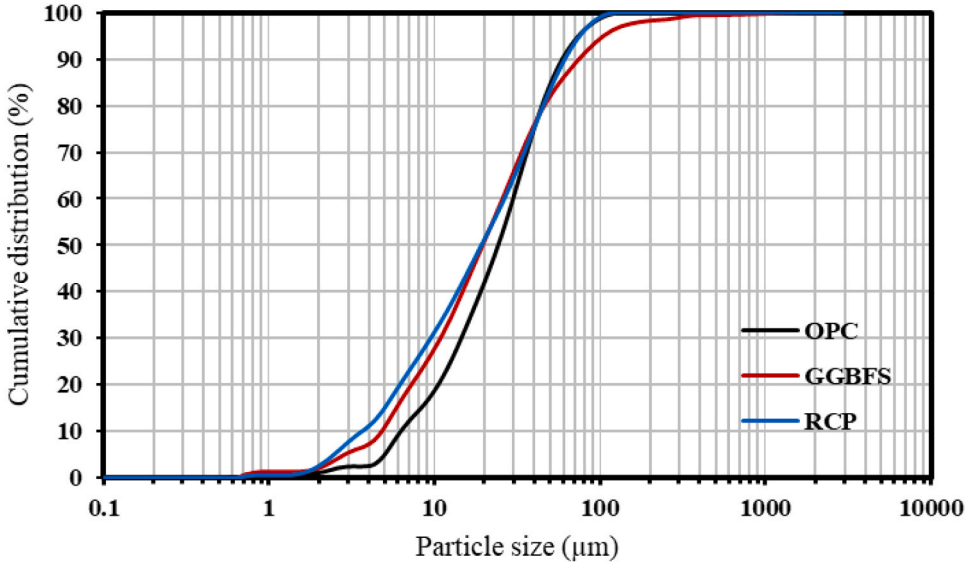

Fig. 10. Particle size distribution of OPC, GGBFS, and RCP.

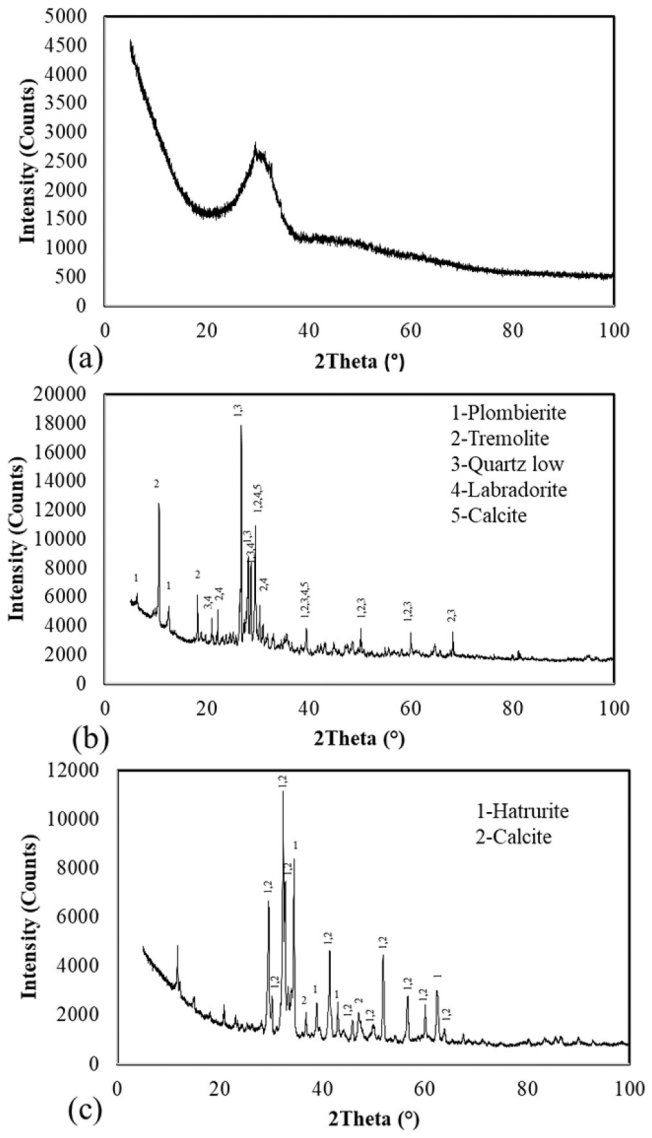

Fig. 11. XRD analysis of (a) GGBFS; (b) RCP; and (c) OPC.

with the P-R-GRO and P-R-GO mixes following consecutively in order.

Table 5 presents the test outcomes investigating the impact of incorporating BF in conventional and eco-friendly concrete on the flexural performance of FRC samples, following ASTM C1609 [79]. Additionally, Fig. 15 displays load-deflection curves of the third-point loading test. A clear 14.7 % increase in flexural tensile strength was observed in F-R-O compared to P-R-O, attributed to the inclusion of BF, which enhanced tensile strength and crack resistance. The reinforcing effect of BF improves bridging action and tension stiffening, enhancing residual strength and toughness. Similarly, F-R-RO, incorporating 15 % RCP, outperformed P-R-RO by a remarkable 30.6 % in flexural tensile strength, attributed to the combined influences of BF and RCP: BF enhanced both tensile strength and crack control, while RCP improved the ITZ between recycled aggregates and the cementitious matrix due to the high fineness and filler effect of RCP [98]. Consequently, F-R-GRO exhibited a substantial 41.4 % increase in flexural tensile strength compared to P-R-GRO, attributed to the improved bond strength between the BF and the surrounding concrete matrix containing SCMs [94].

Concrete mixes with BF exhibited a post-peak tensile softening behavior due to fiber bridging after crack initiation, as seen in Fig. 15(b). FRC mixes incorporating RCP (F-R-RO and F-R-GRO) showed superior post-peak flexural behavior compared to 100 % OPC-based FRC mix (F-R-O). Furthermore, flexural toughness serves as an indicator of concrete's energy absorption capacity, assessing its crack resistance and ductility. This attribute is crucial in applications such as structures exposed to static strains, seismic events, explosive blasts, impact loads, and other dynamic forces [99]. After 28 days, F-R-GRO demonstrated 71 % and 6.9 % higher flexural toughness than F-R-O and F-R-RO, respectively. Residual strengths at L/600, where L is the clear span equivalent to 300 mm, were 59.8 %, 84.3 %, and 79.6 % of ultimate flexural strengths for F-R-O, F-R-RO, and F-R-GRO, respectively. Furthermore, at L/150 deflection, residual strengths were 21.4 %, 35.7 %, and 51.0 % for F-R-O, F-R-RO, and F-R-GRO, respectively. The post-peak flexural properties suggest considerable improvements with the addition of BF to RAC incorporating RCP and GGBFS compared to RAC containing OPC alone. These improvements can be ascribed to the incorporation of pozzolanic materials which contribute to an improved ITZ around the fibers [100]. The improved ITZ between BF and the surrounding matrix contributes to a more stable behavior after the peak, making the concrete more resilient under loading conditions in terms of crack control.

3.5. Workability, density, water absorption, and porosity of concrete

Fig. 16 presents the quantity of superplasticizer needed per cubic meter of concrete to achieve consistent workability within the 65 ± 10 mm range across all concrete mixes. Generally, concrete mixes containing RCA in the P-R-O context required a higher superplasticizer dosage compared to 100 % NGA in the case of P-N-O mix. This can be attributed to the rough surface of RCA particles, causing increased friction and reduced workability. Furthermore, GGBFS-incorporated concrete (P-R-GO) demanded a lower superplasticizer content than P-R-O, attributed to enhanced cementitious particle dispersion and the unique surface characteristics of GGBFS particles, known for their smooth texture and low water absorption [24]. Additionally, RCP-containing concrete required the highest superplasticizer content to achieve equivalent workability, owing to the coarse texture of RCP particles, as evident from SEM images. In contrast, concrete mixes with BF necessitated greater superplasticizer content compared to plain counterparts. The reduction in workability associated with BF inclusion can be attributed to their expanded surface area demanding more cement paste, thus limiting workability. This effect can also be amplified due to moisture absorption by BF and increased fiber-concrete friction during mixing [101].

The water absorption, density, and porosity of all tested concrete mixes are illustrated in Fig. 17(a), Fig. 17(b), and Fig. 17(c), respectively. Notably, consistent trends were observed in water absorption and porosity across all concrete mixes. When considering the influence of aggregate type, incorporating RCA in P-R-O resulted in 7.9 % and 6.7 % higher water absorption and porosity, respectively, compared to P-N-O at 28 days of curing. This outcome can be attributed to the porous adhered mortar of RCA and its greater water absorption relative to NGA [20,94]. Conversely, the density of RAC in P-R-O was 3.1 % lower than the density of conventional concrete in P-N-O, likely due to the higher porosity and lower density of RCA compared to NGA [20]. Regarding the impact of curing duration, both P-R-O and P-N-O exhibited more significant improvements in water absorption, density, and porosity at 90 days of curing than at 28 days. This is attributed to extended cement hydration and the formation of pore-reducing products beyond C-S-H gel.

In the context of binder composition, utilizing GGBFS at 45 % replacement in P-R-GO resulted in an 11.1 % increase in water absorption and a 14.7 % rise in porosity compared to P-R-O at 28 days of curing. After 90 days of curing, P-R-GO displayed a 6.5 % increase in water absorption and a 10.2 % surge in porosity compared to P-R-O, indicating an enhanced microstructure development rate with extended curing using GGBFS. For P-R-RO with 15 % RCP replacement, the

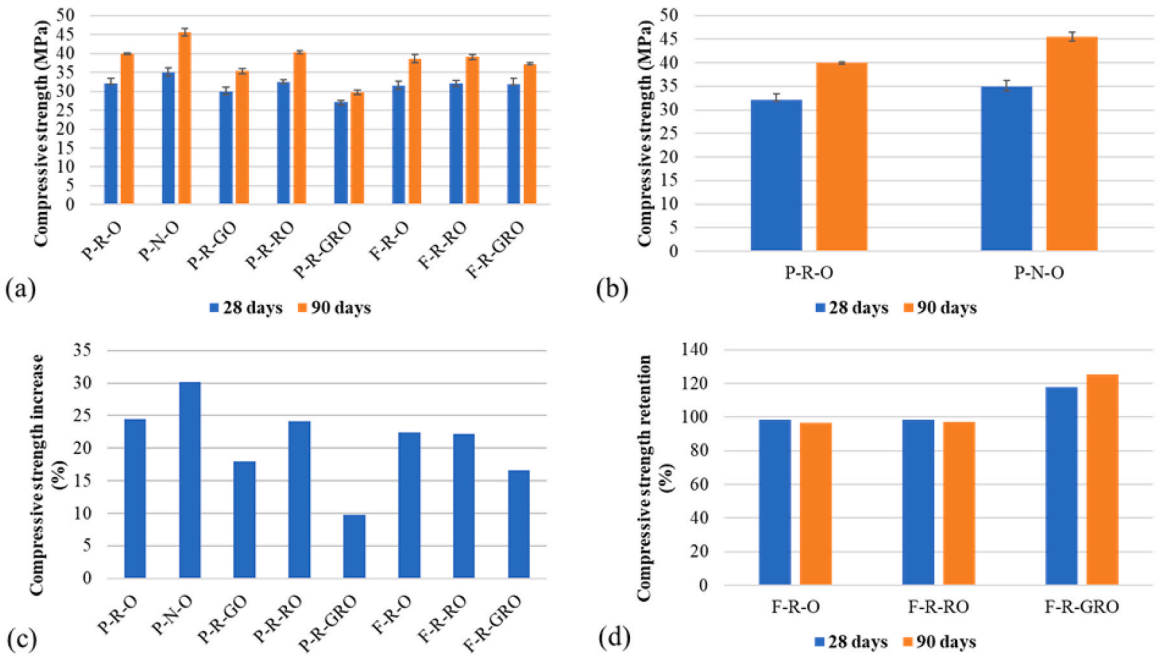

Fig. 12. (a) Compressive strength of concrete mixes used in this study; (b) effect of coarse aggregate type; (c) effect of extended curing of 90 days; and (d) effect of BF incorporation.

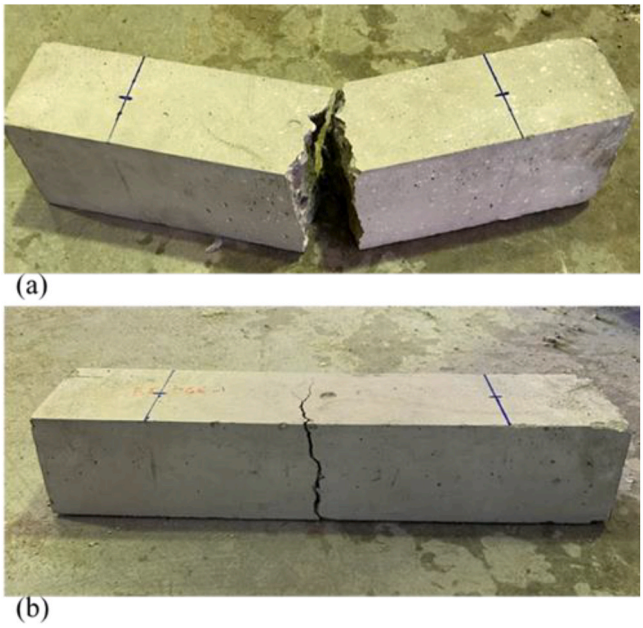

Fig. 13. Post-test images of flexural tensile test prisms (a) plain concrete; and (b) FRC.

concrete exhibited 6.1 % higher water absorption, and 7.2 % greater porosity compared to P-R-O at 28 days of curing. However, with a 90-day curing duration, P-R-RO showed a marginal decrease of 1.9 % in water absorption and 0.9 % in porosity, suggesting negligible variation between P-R-O and P-R-RO. Moreover, the density of P-R-RO surpassed that of P-R-O by 2.3 % and 3.92 % at 28 days and 90 days of curing, respectively. This can be attributed to RCP's filler effect, enhancing concrete packing density and cohesiveness due to its finer particle size compared to cement [102].

Notably, the simultaneous use of GGBFS and RCP as a ternary mix in P-R-GRO yielded 16.6 % higher water absorption and 15.7 % increased

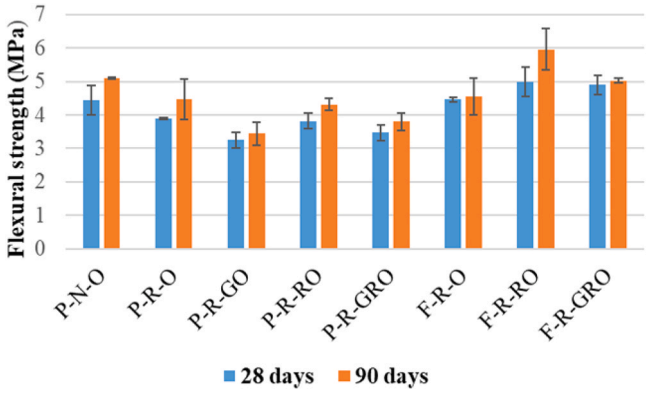

Fig. 14. Flexural tensile strength of different concrete mixes at 28 days and 90 days of curing.

porosity compared to P-R-O at 28 days of curing. At 90 days of curing, P-R-GRO displayed 15.6 % higher water absorption and 14.4 % greater porosity, highlighting consistent reduction rate changes due to prolonged curing. These outcomes stem from lower overall CaO content in binders, GGBFS incorporation being linked to higher autogenous shrinkage [103,104], contributing to increased cracking, water absorption, and porosity, as well as lower density compared to P-R-O.

When evaluating the impact of fibers on water absorption, porosity, and density, two key factors emerge: (1) the introduction of fibers creates additional ITZs, elevating water absorption and porosity; (2) fiber addition reduces drying shrinkage [105] and autogenous shrinkage [104], limiting microcracks and thus lowering water absorption and porosity. After 28 days of curing, water absorption increased by approximately 6.8 %, from 6.6 % in P-R-O to 7.0 % in F-R-O. Similarly, porosity exhibited a rise of around 7.2 %, from 14.9 % to 16.0 % with BF, indicating a more pronounced influence of added ITZ due to fibers' presence.

In contrast, water absorption decreased by about 5.0 %, from 7.0 % in P-R-RO to 6.7 % in F-R-RO. Similarly, porosity decreased by approximately 4.2 %, from 16.0 % to 15.4 % with the inclusion of BF.

Table 5
Flexural tensile properties of plain concrete and FRC prisms.

Mix designation	***P1*** (kN)	***δ1*** (mm)	***P_p(28d)*** (kN)	***δ_p*** (mm)	***PD600*** (kN)	***PD150*** (kN)	***TD150*** (J)	***P_p(90d)*** (kN)
F-R-O	14.850	0.061	14.850	0.062	8.880	3.175	13.105	15.143
F-R-RO	15.320	0.068	16.617	0.078	14.003	5.923	20.957	19.873
F-R-GRO	16.280	0.069	16.330	0.073	13.000	8.335	22.410	16.745
P-N-O	-	-	14.770	0.041	-	-	-	17.030
P-R-O	-	-	12.950	0.048	-	-	-	14.890
P-R-GO	-	-	10.820	0.042	-	-	-	11.490
P-R-RO	-	-	12.730	0.060	-	-	-	14.370
P-R-GRO	-	-	11.550	0.042	-	-	-	12.650

* ***P1***: Cracking load; ***δ1***: deflection corresponding to cracking load; ***P_p(28d)***: peak load at 28 days; ***P_p(90d)***: peak load at 90 days; ***δ_p***: deflection corresponding to peak load; ***PD600***: residual load at L/600 deflection; ***PD150***: residual load at L/150 deflection; and ***TD150***: flexural toughness (Area under the load vs. displacement curve from 0 up to L/150 deflection)

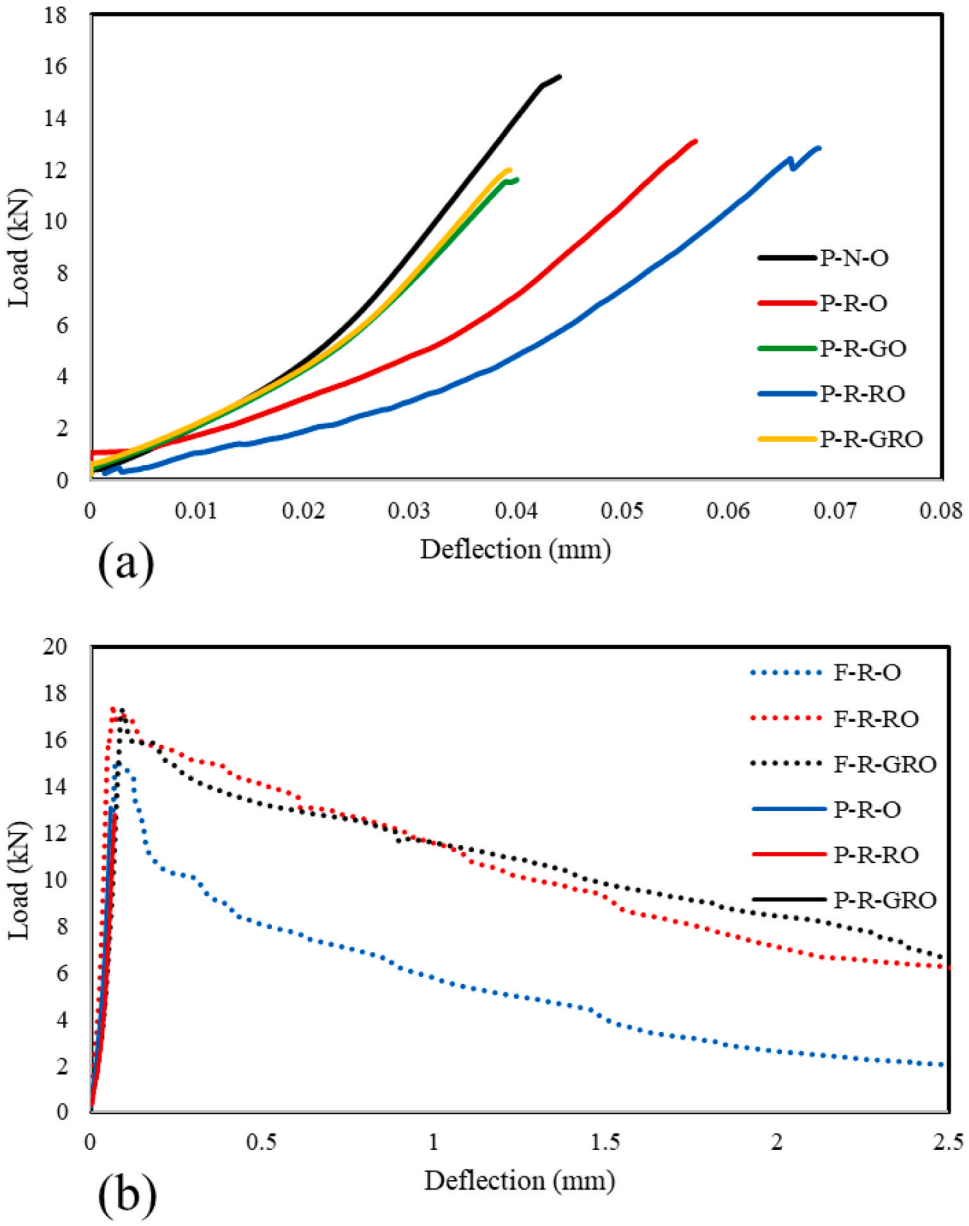

Fig. 15. Load-deflection curves of flexural tensile test: (a) plain concrete specimens; and (b) plain and their counterparts FRC specimens.

Furthermore, water absorption exhibited a decrease of approximately 9.1 %, from 7.7 % in P-R-GRO to 7.0 % in F-R-GRO. Correspondingly, porosity reduced by about 6.7 %, from 17.3 % to 16.1 %, upon introducing BF. This suggests that fibers have the ability to counteract ITZ effects through crack restraint. These variations highlight the role of mix composition, encompassing RCP and GGBFS, in shaping fiber

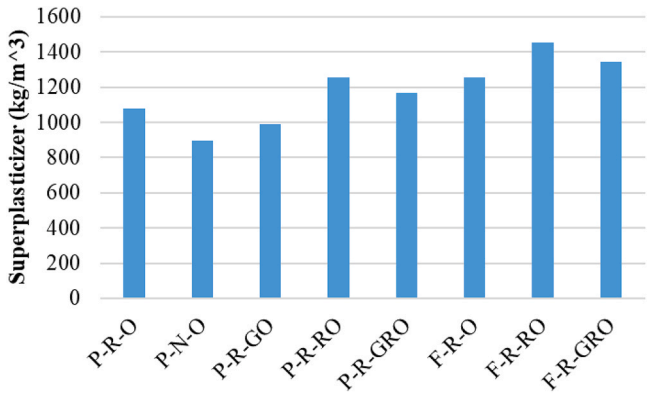

Fig. 16. Superplasticizer quantity required to maintain comparable workability for all mixes.

impact on water absorption and porosity. Notably, BF addition had negligible effects on density, with variations within 5 %. The most notable density change occurred in F-R-GRO, revealing a minor 4.9 % increase over P-R-GRO due to the porosity-reducing capacity of the fibers. Furthermore, the density in FRC showed no significant alteration with extended curing duration.

3.6. Rapid chloride penetration test analysis

Fig. 18 illustrates the impact of the investigated parameters on evaluating concrete's resistance to chloride penetration using the RCPT. The measurement of total charge passing through concrete specimens serves as an indicator of chloride penetration. After 28 days of curing, the P-R-O specimens incorporating RCA exhibited a total charge of 1803 coulombs, while P-N-O specimens with NGA yielded a total charge of 1785 coulombs, representing a negligible variation in terms of chloride penetration. This observation suggests that aggregate size countered the effect of adhered mortar on RCA, with finer aggregates introducing more ITZ conducive to higher chloride ion ingress[106]. Upon extending curing to 90 days, P-R-O's total charge passed was 20.7 % higher than that of P-N-O. This distinction can be attributed to P-N-O's lower porosity and accelerated hydration rate during extended curing. The higher rate of compressive strength increases in P-N-O (30 %) compared to P-R-O (24.5 %) when extending curing from 28 to 90 days further supports this finding.

Furthermore, the incorporation of GGBFS in concrete, particularly in the case of P-R-GO, resulted in a total charge of 1014 coulombs at 28 days of curing and 417 coulombs after 90 days of curing. This significant reduction in the total charge passed offset the potential decline in chloride resistance associated with the use of RCA. Notably, P-R-GO consistently outperformed P-R-O, exhibiting superior chloride resistance. At 28 days, P-R-GO fell within the "Low" category for chloride ion penetrability, while at 90 days, it was categorized as "Very Low". The total charge passed for P-R-GO was 43.8 % lower at 28 days and 54.1 %

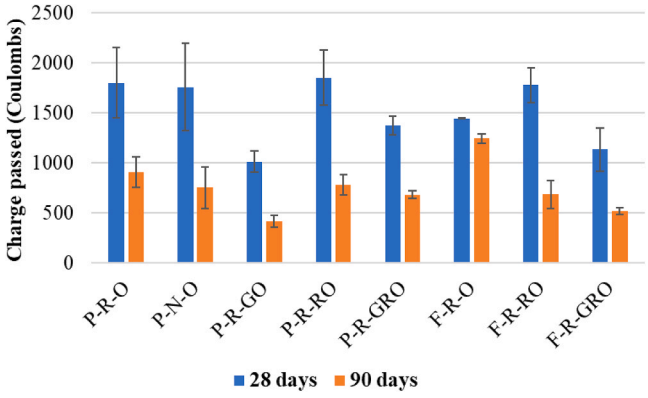

Fig. 18. Total charge passed by RCPT for all concrete mixes used in this study.

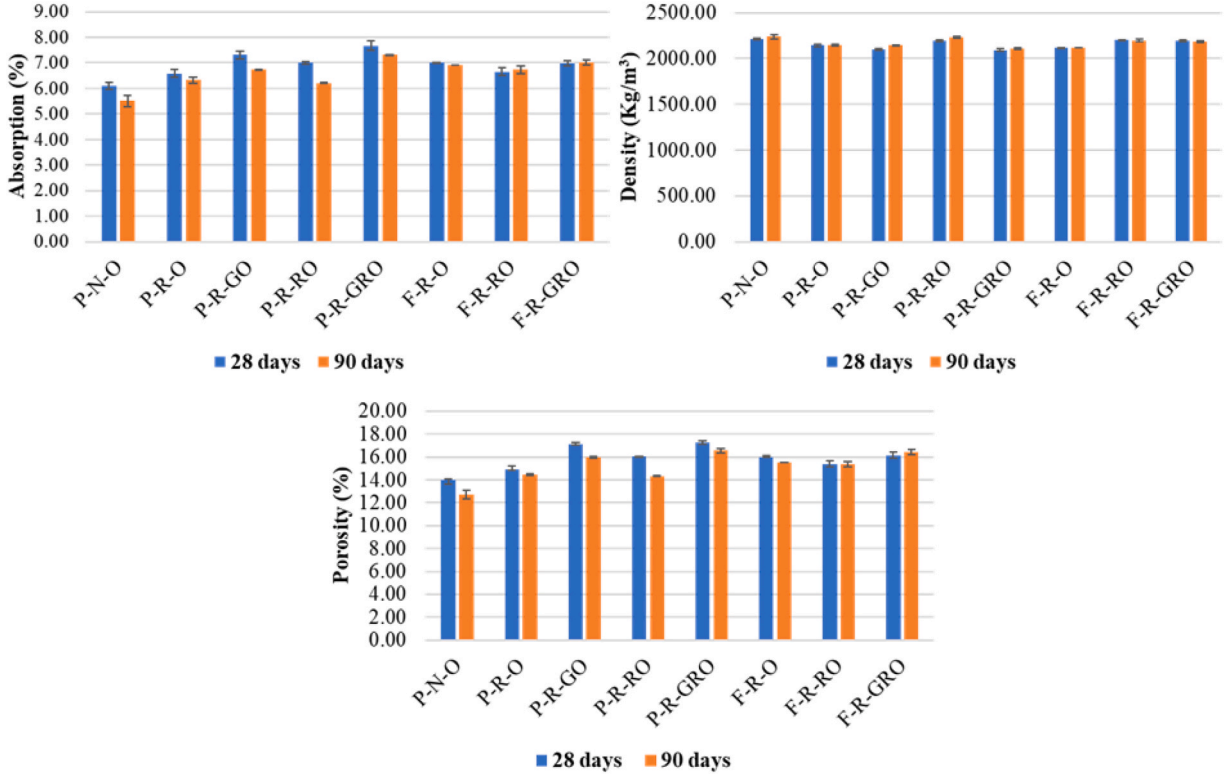

Fig. 17. (a) Concrete water absorption; (b) concrete density; and (c) concrete porosity.

lower at 90 days compared to P-R-O. Introducing RCP as a 15 % replacement for OPC in P-R-RO resulted in a total charge of 1851 coulombs at 28 days of curing and 781 coulombs at 90 days of curing. This suggests comparable chloride ion penetration at 28 days and notably lower chloride ion penetration at 90 days compared to P-R-O. The total charge passed for P-R-RO was 2.7 % higher at 28 days and 14.1 % lower at 90 days compared to P-R-O. Furthermore, combining RCP and GGBFS in the case of P-R-GRO enhanced chloride resistance. At 28 days, P-R-GRO exhibited a total charge of 1379 coulombs, and at 90 days, it recorded 682 coulombs, indicating a 23.5 % reduction at 28 days and 25.0 % reduction at 90 days compared to P-R-O. These findings underscore the positive impact of incorporating GGBFS and RCP in concrete mixes, enhancing chloride resistance compared to P-R-O. These results highlight the potential of SCMs and recycled concrete components for enhancing concrete durability in terms of chloride penetration resistance, attributed to the lower permeability compared to OPC concrete. This outcome aligns with the expected result of the pozzolanic reaction, leading to denser microstructures. It is important to note that while GGBFS concrete and OPC concrete may exhibit comparable total porosities, however, the pore structures in GGBFS incorporating concrete tend to be finer [107].

The incorporation of BF in concrete, particularly F-R-O with 100 % OPC, resulted in a reduced total charge passed of 1444 coulombs at 28 days, compared to 1803 coulombs in the case of P-R-O, indicating improved chloride resistance. The total charge passed for F-R-O was approximately 19.9 % lower than P-R-O at 28 days. Furthermore, the combined effect of SCM and BF further improved chloride resistance. For F-R-GRO specimen, the total charge passed was 1134 coulombs at 28 days, compared to 1379 coulombs for P-R-GRO, indicating a 17.8 % lower total charge. Additionally, F-R-RO exhibited better performance with a total charge passed of 1781 coulombs at 28 days, compared to 1851 coulombs for P-R-RO indicating 3.80 % lower total charge passed. This suggests a slight improvement in chloride resistance when incorporating BF with RCP. This can be ascribed to the ability of BF to disrupt the interconnectivity of the porous network in concrete, subsequently contributing to the reduced permeability and improved chloride

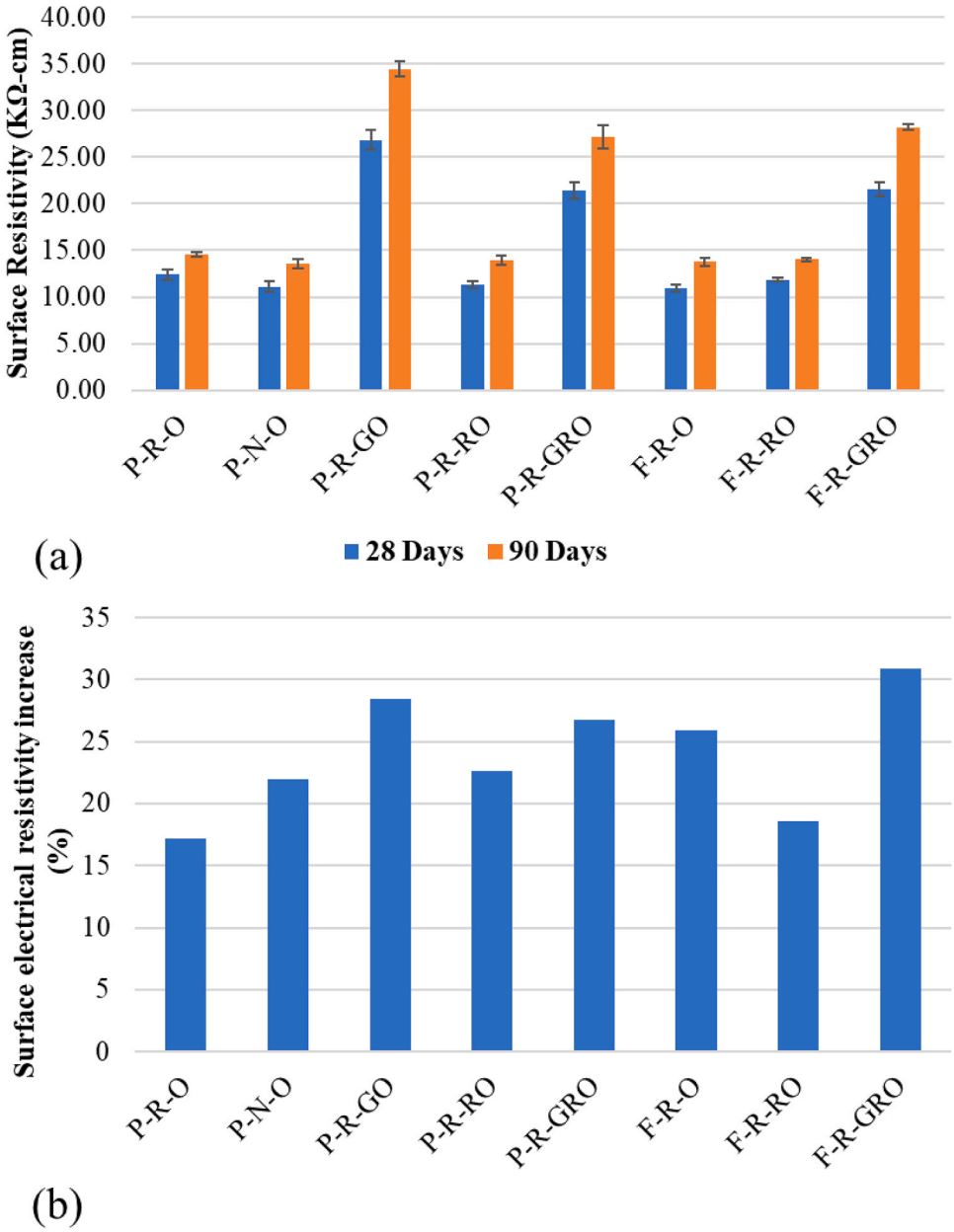

Fig. 19. (a) SER results for specimens in this study; and (b) effect of 90 days curing on SER.

resistance [108]. The addition of BF did not disrupt the enhancement of chloride resistance with extended curing, continuing to outperform plain green concrete incorporating SCMs. These findings highlight the beneficial impact of incorporating BF in concrete mixes, leading to a reduction in chloride penetration and improved durability.

3.7. Surface electrical resistivity

In this study, the SER test was employed to improve results repeatability compared to RCPT. Moreover, the test can be used as an indicator for the changes in the concrete pore structure over time and tends to strongly correlate with the water permeability of concrete incorporating traditional SCMs [109]. Fig. 19 illustrates the SER of concrete mixes at both 28 and 90 days of curing. Analyzing the impact of aggregates, Fig. 19(a) reveals that incorporating 50 % RCA in P-R-O had no significant effect on SER compared to 100 % NGA in P-N-O, indicating comparable chloride resistance. This trend was also observed with a 25 % RCA partial replacement in Sasanipour and Aslani study [110]. This can be attributed to RCA gradation, where larger aggregates dominated the 5 mm to 10 mm ratio compared to NGA. Larger aggregates typically elevate electrical resistivity, slowing current flow around aggregates through the porous ITZ when larger surface area aggregates are present [111]. At 28 days, P-N-O exhibited SER of 11.1 KΩ cm, categorized as "high" chloride ion penetration, while P-R-O showed 12.4 KΩ-cm, "moderate" as per AASHTO TP 95–11 [80]. After 90 days, SER increased by 21.9 % for P-N-O and 17.1 % for P-R-O due to continued cement hydration, maintaining a "moderate" classification in terms of chloride ion penetration.

Additionally, considering the binder composition effects, the SER in P-R-GO with 45 % GGBFS, was notably higher, measuring 116.1 % higher SER than that of P-R-O, containing 100 % OPC. As a result, the P-R-GO blend was categorized as having “Low” chloride ion penetration susceptibility following AASHTO TP 95–11 [80]. This substantial increase in SER can be attributed to the presence of GGBFS, which enhanced the capillary tortuosity of the concrete while diminishing the ionic concentration within the concrete pore solution [112]. Moreover, the rate of SER escalation over the 28-day to 90-day curing period was notably higher for P-R-GO (28.5 %) than for P-R-O (17.2 %), as depicted in Fig. 19(b). With the introduction of a 15 % RCP replacement, minor declines in SER by 8.6 % and 4.4 % were evident at 28 days and 90 days of curing, respectively, compared to P-R-O. This decrease could be attributed to the heightened interconnectivity within the concrete pore system following RCP incorporation. However, with an extended 90-day curing duration, the SER reduction in P-R-RO was less pronounced than that at 28 days, possibly due to hydrated products replenishing the voids and decreasing the degree of pore system interconnectivity. Similar observations were made by Horsakulthai [42]. The synergistic effect of RCP and GGBFS on RAC (P-R-GRO) significantly enhanced its SER values, which were 72.8 % and 87 % higher than those of P-R-O at 28 and 90 days of curing, respectively. Furthermore, the SER of P-R-GRO exhibited a 26.7 % increase from 28 to 90 days of curing, demonstrating a higher rate of SER development compared to P-R-O (17.2 %).

Regarding incorporating BF into the concrete blends, particularly in the 100 % OPC concrete mixture like F-R-O, BF resulted in an 11.8 % reduction in SER compared to P-R-O after 28 days. This reduction can be ascribed to the increased concrete porosity indicated by the conducted tests in this study. However, as curing extended to 90 days, the SER reduction in F-R-O became nearly negligible, presenting a 5.3 % lower SER than that of P-R-O. Conversely, when BF was integrated into the concrete mix containing both GGBFS and RCP, as seen in F-R-RO and F-R-GRO, the effect of BF incorporation yielded minimal impact, resulting in a slight SER increase. This outcome can be attributed to the combined use of BF and SCMs leading to reduced porosity in the concrete due to the ability of BF to restrict internal cracks of concrete associated with temperature shrinkage and autogenous shrinkage. Additionally, the influence of fibers became more prominent with the extended 90-day curing duration in the case of F-R-GRO, likely due to the higher hydration rate during prolonged curing, leading to increased C-S-H formation, reduction in capillary pores, and enhancement of the concrete pore structure [113].

3.8. SEM analysis

Microstructural analysis conducted through SEM provides valuable insights into concrete quality and durability, detecting defects like voids, cracks, and poorly bonded interfaces. Fig. 20 displays the microstructure of different plain concrete specimens examined in this study following a 28-day curing period. In Fig. 20(a), the pores within the cementitious matrix of P-N-O exhibited a more uniformly distributed pattern, with relatively smaller sizes compared to the other specimens. This observation potentially accounts for the superior mechanical performance observed in P-N-O compared to the other plain concrete mixes. Furthermore, the inclusion of 15 % RCP in the P-R-RO mix resulted in a microstructure with larger macropores and fewer micropores, as evident in Fig. 20(d), contrasting with the microstructure of 100 % OPC-based P-R-O in Fig. 20(b). Similarly, both P-R-GO and P-R-GRO exhibited non-uniform pore distribution localized within specific regions of the concrete mortar, as depicted in Fig. 20(c) and Fig. 20(e), respectively. Such uneven pore distribution could contribute to strength variations across different sections of the cementitious mixture [114].

Additionally, Fig. 21 provides higher magnifications of the concrete pastes, facilitating the identification of hydration products and pore interconnectivity. In Fig. 21(a), the microstructure of mix P-R-O exhibited uninterrupted voids with straight pathways devoid of hydration products intrusion. Likewise, for P-R-RO, the microstructure showcases a similar pattern of cracks and voids, albeit wider compared to P-R-O. On the other hand, Figs. 21(c) and 21(d) depict a different scenario for P-R-GO and P-R-GRO. These mixes incorporating GGBFS show the presence of hydration products disrupting the interconnectivity of porous network alongside pathways with higher tortuosity when contrasted with concrete containing 100 % OPC. This observation potentially explains the significantly enhanced chloride resistance and elevated electrical resistivity noticed in P-R-GO and P-R-GRO, surpassing the performance of P-N-O, P-R-O, and P-R-RO.

In general, the primary hydration product in concrete is C-S-H, which imparts strength and durability. The introduction of GGBFS initiates a reaction with water and calcium hydroxide (CH), generating additional calcium silicate hydrate (C-S-H) gel, which fills the voids, densifying the microstructure and decreasing pore connectivity. Additionally, GGBFS, containing alumina, reacts with calcium hydroxide to produce calcium aluminate hydrate (C-A-H) compounds. These compounds actively engage in the hydration process, effectively occupying pore spaces and further disrupting their connectivity. Moreover, GGBFS promotes the formation of ettringite, a calcium aluminum sulfate hydrate compound that precipitates and fills voids, thus impeding fluid movement and diminishing interconnectivity within the concrete matrix. The presence of these hydration products, evident in Fig. 21(c) and Fig. 21(d), effectively reduces permeability by blocking pores and disturbing their interconnectivity [115]. This mechanism contributes to the enhanced durability and long-term performance of concrete through the incorporation of GGBFS.

4. Conclusion

This study examined the influence of basalt fibers (BF) and partial replacement of ordinary Portland cement (OPC) with recycled concrete powder (RCP), and ground granulated blast furnace slag (GGBFS) on the mechanical and durability attributes of recycled aggregate concrete (RAC) incorporating 50 % recycled concrete aggregates (RCA) by direct volume replacement of natural gabbro aggregates (NGA). The following key conclusions can be drawn:

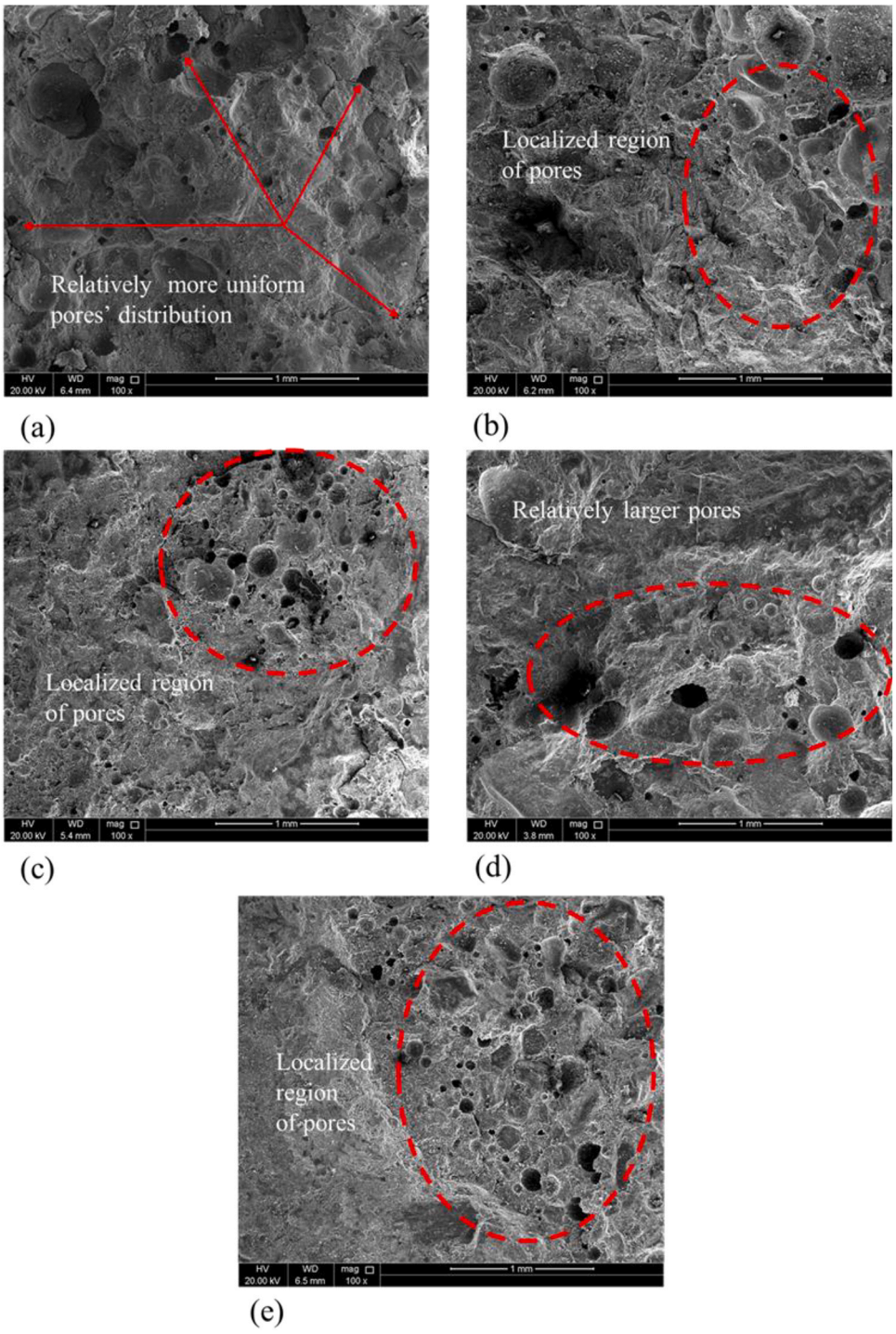

Fig. 20. SEM images of (a) P-N-O; (b) P-R-O; (c) P-R-GO; (d) P-R-RO; and (e) P-R-GRO.

1. RAC with 50 % RCA replacement showed a reduction of 8.3 % and 12.3 % in compressive strength at 28 and 90 days of curing, respectively, compared to conventional concrete with 100 % NGA. Additionally, incorporating 15 % RCP in RAC maintained comparable compressive strength compared to 100 % OPC-based RAC. However, ternary blended RAC comprising 15 % RCP, 30 % GGBFS, and 55 % OPC demonstrated reductions of 15.6 % and 25.6 % at 28 and 90 days of curing, respectively, relative to RAC with 100 % OPC, but adding 0.75 % BF mitigated these reductions, aligning compressive strength with 100 % OPC-based RAC, with and without BF, across all curing durations.
2. The use of 50 % RCA replacement resulted in an 11.9 % decrease in flexural tensile strength compared to concrete containing 100 % NGA. Furthermore, binary blended RAC comprising 15 % RCP and 85 % OPC exhibited comparable flexural tensile strength to that of 100 % OPC-based RAC, while ternary blended RAC experienced a 10.8 % reduction. Notably, the binary blended basalt fiber reinforced recycled aggregate concrete (BFRRAC) comprising 15 % RCP and 85 % OPC achieved the highest flexural tensile strength, surpassing 100 % OPC-based BFRRAC. Additionally, ternary blended BFRRAC comprising 15 % RCP, 30 % GGBFS, and 55 % OPC showed around

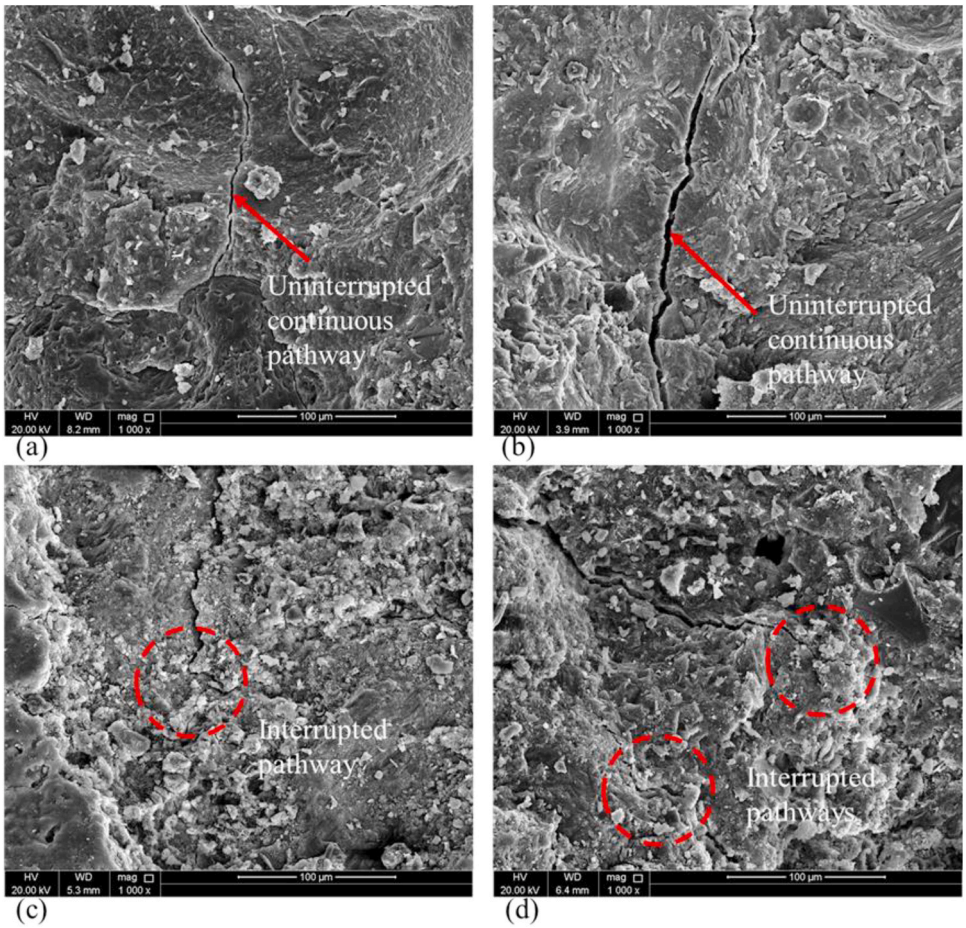

Fig. 21. SEM images of: (a) P-R-O; (b) P-R-RO; (c) P-R-GO; and (d) P-R-GRO.

10 % higher flexural tensile strength compared to 100 % OPC-based BFRRAC, along with the highest flexural toughness.

3. Binary blended RAC comprising 15 % RCP and 85 % OPC experienced a decline in concrete workability, whereas the use of GGBFS improved the workability of RAC compared to 100 % OPC-based RAC.
4. Ternary blended RAC exhibited a 16.6 % increase in water absorption and a 15.7 % increase in porosity relative to 100 % OPC-based RAC; However, the addition of BF mitigated these effects. Ternary blended RAC demonstrated 23.5 % lower charge passing during the rapid chloride penetration test compared to 100 % OPC-based RAC. with further reductions of 20.2 % and 24.1 % observed at 28 and 90 days of curing, respectively, upon incorporating 0.75 % BF.
5. Surface electrical resistivity (SER) measurements indicated negligible impact with 50 % RCA replacement compared to respective concrete with 100 % NGA. Binary blended RAC of 45 % GGBFS and 55 % OPC displayed the highest SER among the tested specimens. Ternary blended RAC exhibited SER values 73.0 % and 87.0 % higher than 100 % OPC-based RAC after 28 days and 90 days of curing, respectively. BF addition had no significant effect on SER.
6. Microstructural analysis through SEM revealed that ternary blended RAC demonstrated disrupted interconnectivity of concrete porous network and increased tortuosity. This, in turn, enhanced chloride resistance and reduced permeability of concrete.

These findings demonstrate the potential of using RCP, GGBFS, and BF to enhance the mechanical and durability performance of RAC. It is imperative to underscore that the findings remain constrained to the impacts of the parameters investigated within this research study. However, further research is necessary to explore varying combinations and replacement ratios of RCP and GGBFS for optimal mix design. Moreover, long-term curing beyond 90 days should be considered for future investigations. Additionally, large-scale evaluations of reinforced concrete beams made with ternary blended RAC incorporating RCP should be conducted to assess shear and flexural behavior comprehensively.

CRediT authorship contribution statement

Wael I. Alnahhal: Writing – review & editing, Supervision, Project administration, Methodology, Funding acquisition, Conceptualization. **Alaa Taha:** Writing – original draft, Validation, Methodology, Formal analysis, Data curation, Conceptualization.

Declaration of Competing Interest

The authors declare that they have no known competing financial interests or personal relationships that could have appeared to influence the work reported in this paper.

Acknowledgments

The authors express their appreciation for the financial support provided by GSRA grant number GSRA7-1-0419-20019, from Qatar National Research Fund (QNRF), an entity affiliated with the Qatar Foundation, and by QUPD-CENG-24/25-1410 from Qatar University. Open Access funding was provided by the Qatar National Library. Moreover, the authors would like to express their gratitude to QPMC and

Aljabor Cement Industries for their support in providing some of the materials used in this research. It is important to note that the conclusions derived from this study are, exclusively, the responsibility of the authors.

Appendix A. Supporting information

Supplementary data associated with this article can be found in the online version at doi:10.1016/j.istruc.2024.108058.

References

[1] Gartner E. Industrially interesting approaches to "low-CO2" cements. Cem Concr Res 2004. https://doi.org/10.1016/j.cemconres.2004.01.021.

[2] Scrivener KL, Kirkpatrick RJ. Innovation in use and research on cementitious material. Cem Concr Res 2008. https://doi.org/10.1016/j.cemconres.2007.09.025.

[3] Pacheco-Torgal F, Jalali S. Cementitious building materials reinforced with vegetable fibres: a review. Constr Build Mater 2011. https://doi.org/10.1016/j.conbuildmat.2010.07.024.

[4] Freedonia. World construction aggregates - market size, market share, market leaders, demand forecast, sales, company profiles, market research, industry trends and companies 2015. ⟨https://www.freedoniagroup.com/industry-study/world-construction-aggregates-2838.htm⟩.

[5] Gagg CR. Cement and concrete as an engineering material: an historic appraisal and case study analysis. Eng Fail Anal 2014. https://doi.org/10.1016/j.engfailanal.2014.02.004.

[6] Xiao J, Ma Z, Sui T, Akbarnezhad A, Duan Z. Mechanical properties of concrete mixed with recycled powder produced from construction and demolition waste. J Clean Prod 2018. https://doi.org/10.1016/j.jclepro.2018.03.277.

[7] Cantero B, Bravo M, de Brito J, Sáez del Bosque IF, Medina C. Mechanical behaviour of structural concrete with ground recycled concrete cement and mixed recycled aggregate. J Clean Prod 2020;275:122913. https://doi.org/10.1016/j.jclepro.2020.122913.

[8] Lotfi S, Deja J, Rem P, Mróz R, Van Roekel E, Van Der Stelt H. Mechanical recycling of EOL concrete into high-grade aggregates. Resour Conserv Recycl 2014. https://doi.org/10.1016/j.resconrec.2014.03.010.

[9] Kurda R, de Brito J, Silvestre JD. Influence of recycled aggregates and high contents of fly ash on concrete fresh properties. Cem Concr Compos 2017. https://doi.org/10.1016/j.cemconcomp.2017.09.009.

[10] Brand AS, Roesler JR, Salas A. Initial moisture and mixing effects on higher quality recycled coarse aggregate concrete. Constr Build Mater 2015. https://doi.org/10.1016/j.conbuildmat.2015.01.047.

[11] Etxeberria M, Vázquez E, Marí A, Barra M. Influence of amount of recycled coarse aggregates and production process on properties of recycled aggregate concrete. Cem Concr Res 2007. https://doi.org/10.1016/j.cemconres.2007.02.002.

[12] Xiao J, Li J, Zhang C. Mechanical properties of recycled aggregate concrete under uniaxial loading. Cem Concr Res 2005. https://doi.org/10.1016/j.cemconres.2004.09.020.

[13] Gesoglu M, Güneyisi E, Öz HÖ, Taha I, Yasemin MT. Failure characteristics of self-compacting concretes made with recycled aggregates. Constr Build Mater 2015. https://doi.org/10.1016/j.conbuildmat.2015.08.036.

[14] Kong D, Lei T, Zheng J, Ma C, Jiang J, Jiang J. Effect and mechanism of surface-coating pozzalanics materials around aggregate on properties and ITZ microstructure of recycled aggregate concrete. Constr Build Mater 2010. https://doi.org/10.1016/j.conbuildmat.2009.10.038.

[15] Katz A. Properties of concrete made with recycled aggregate from partially hydrated old concrete. Cem Concr Res 2003. https://doi.org/10.1016/S0008-8846(02)01033-5.

[16] Kou SC, Poon CS, Agrela F. Comparisons of natural and recycled aggregate concretes prepared with the addition of different mineral admixtures. Cem Concr Compos 2011. https://doi.org/10.1016/j.cemconcomp.2011.05.009.

[17] Beltrán MG, Barbudo A, Agrela F, Galvín AP, Jiménez JR. Effect of cement addition on the properties of recycled concretes to reach control concretes strengths. J Clean Prod 2014. https://doi.org/10.1016/j.jclepro.2014.05.053.

[18] Silva RV, De Brito J, Dhir RK. Establishing a relationship between modulus of elasticity and compressive strength of recycled aggregate concrete. J Clean Prod 2016. https://doi.org/10.1016/j.jclepro.2015.10.064.

[19] Wang B, Yan L, Fu Q, Kasal B. A comprehensive review on recycled aggregate and recycled aggregate concrete. Resour Conserv Recycl 2021;171:105565. https://doi.org/10.1016/j.resconrec.2021.105565.

[20] Ozbakkaloglu T, Gholampour A, Xie T. Mechanical and durability properties of recycled aggregate concrete: effect of recycled aggregate properties and content. J Mater Civ Eng 2018;30:04017275. https://doi.org/10.1061/(asce)mt.1943-5533.0002142.

[21] Ho NY, Lee YPK, Lim WF, Zayed T, Chew KC, Low GL, et al. Efficient utilization of recycled concrete aggregate in structural concrete. J Mater Civ Eng 2013;25:318–27. https://doi.org/10.1061/(asce)mt.1943-5533.0000587.

[22] Juenger MCG, Snellings R, Bernal SA. Supplementary cementitious materials: new sources, characterization, and performance insights. Cem Concr Res 2019;122:257–73. https://doi.org/10.1016/j.cemconres.2019.05.008.

[23] Zhuang XY, Chen L, Komarneni S, Zhou CH, Tong DS, Yang HM, et al. Fly ash-based geopolymer: clean production, properties and applications. J Clean Prod 2016. https://doi.org/10.1016/j.jclepro.2016.03.019.

[24] Megat Johari MA, Brooks JJ, Kabir S, Rivard P. Influence of supplementary cementitious materials on engineering properties of high strength concrete. Constr Build Mater 2011. https://doi.org/10.1016/j.conbuildmat.2010.12.013.

[25] Elahi A, Basheer PAM, Nanukuttan SV, Khan QUZ. Mechanical and durability properties of high performance concretes containing supplementary cementitious materials. Constr Build Mater 2010. https://doi.org/10.1016/j.conbuildmat.2009.08.045.

[26] Oner A, Akyuz S. An experimental study on optimum usage of GGBS for the compressive strength of concrete. Cem Concr Compos 2007. https://doi.org/10.1016/j.cemconcomp.2007.01.001.

[27] Rafieizonooz M, Mirza J, Salim MR, Hussin MW, Khankhaje E. Investigation of coal bottom ash and fly ash in concrete as replacement for sand and cement. Constr Build Mater 2016;116:15–24. https://doi.org/10.1016/j.conbuildmat.2016.04.080.

[28] McCarthy MJ, Robl T, Csetenyi LJ. Recovery, processing, and usage of wet-stored fly ash. Coal combustion products (CCPs): characteristics, utilization and beneficiation. Woodhead Publishing; 2017. p. 343–67. https://doi.org/10.1016/B978-0-08-100945-1.00014-9.

[29] Scrivener KL, John VM, Gartner EM. Eco-efficient cements: potential economically viable solutions for a low-CO2 cement-based materials industry. Cem Concr Res 2018;114:2–26. https://doi.org/10.1016/j.cemconres.2018.03.015.

[30] Sharma R, Khan RA. Effect of different supplementary cementitious materials on mechanical and durability properties of concrete. J Mater Eng Struct 2016.

[31] 96/04917 The influence of high early-strength (HES) mineralized clinker on the strength of development of blended cements containing fly ash, slag, or ground limestone. Fuel Energy Abstr 1996. https://doi.org/10.1016/0140-6701(96)89649-4.

[32] Saraya MESI. Study physico-chemical properties of blended cements containing fixed amount of silica fume, blast furnace slag, basalt and limestone, a comparative study. Constr Build Mater 2014. https://doi.org/10.1016/j.conbuildmat.2014.08.071.

[33] Zhang MH, Malhotra VM. Characteristics of a thermally activated alumino-silicate pozzolanic material and its use in concrete. Cem Concr Res 1995. https://doi.org/10.1016/0008-8846(95)00167-0.

[34] Boukendakdji O, Kadri EH, Kenai S. Effects of granulated blast furnace slag and superplasticizer type on the fresh properties and compressive strength of self-compacting concrete. Cem Concr Compos 2012. https://doi.org/10.1016/j.cemconcomp.2011.08.013.

[35] Bilim C, Atiş CD, Tanyildizi H, Karahan O. Predicting the compressive strength of ground granulated blast furnace slag concrete using artificial neural network. Adv Eng Softw 2009. https://doi.org/10.1016/j.advengsoft.2008.05.005.

[36] Khatib JM, Hibbert JJ. Selected engineering properties of concrete incorporating slag and metakaolin. Constr Build Mater 2005. https://doi.org/10.1016/j.conbuildmat.2004.07.017.

[37] Chen HJ, Huang SS, Tang CW, Malek MA, Ean LW. Effect of curing environments on strength, porosity and chloride ingress resistance of blast furnace slag cement concretes: a construction site study. Constr Build Mater 2012. https://doi.org/10.1016/j.conbuildmat.2012.06.052.

[38] Teng S, Lim TYD, Sabet Divsholi B. Durability and mechanical properties of high strength concrete incorporating ultra fine ground granulated blast-furnace slag. Constr Build Mater 2013. https://doi.org/10.1016/j.conbuildmat.2012.11.052.

[39] Tang Q, Ma Z, Wu H, Wang W. The utilization of eco-friendly recycled powder from concrete and brick waste in new concrete: a critical review. Cem Concr Compos 2020. https://doi.org/10.1016/j.cemconcomp.2020.103807.

[40] Gupta T, Siddique S, Sharma RK, Chaudhary S. Behaviour of waste rubber powder and hybrid rubber concrete in aggressive environment. Constr Build Mater 2019. https://doi.org/10.1016/j.conbuildmat.2019.05.080.

[41] Hou Y, Yu Z, Zhang J, Yang H, Song W. Gray model study of strength and pore structure of recycled concrete powder (RCP) concrete based on low-field NMR technology. Materials 2023;16:6058. https://doi.org/10.3390/ma16176058.

[42] Horsakulthai V. Effect of recycled concrete powder on strength, electrical resistivity, and water absorption of self-compacting mortars. Case Stud Constr Mater 2021;15:e00725. https://doi.org/10.1016/j.cscm.2021.e00725.

[43] Zhang J, Zhou ZH, Cheng X. Formation kinetics of regenerated cement clinker calcined by using wasted recycling concrete powders as raw meals. Adv Mat Res 2014. https://doi.org/10.4028/www.scientific.net/amr.1073-1076.1309.

[44] Tian F, Xie XS, Hu WX. Research on cement pulverized admixture of waste concrete powder. Adv Mat Res 2011. https://doi.org/10.4028/www.scientific.net/AMR.194-196.759.

[45] Kirgiz MS. Characteristic properties of marble and brick powders. Adv Mat Res 2013. https://doi.org/10.4028/www.scientific.net/AMR.749.483.

[46] Santhosh AM, Thomas A. Experimental studies on brick powder replaced concrete exposed to elevated temperature. Lect Notes Civ Eng 2020. https://doi.org/10.1007/978-3-030-26365-2_4.

[47] O'Farrell M, Wild S, Sabir BB. Pore size distribution and compressive strength of waste clay brick mortar. Cem Concr Compos 2001. https://doi.org/10.1016/S0958-9465(00)00070-6.

[48] Qian D, Yu R, Shui Z, Sun Y, Jiang C, Zhou F, et al. A novel development of green ultra-high performance concrete (UHPC) based on appropriate application of recycled cementitious material. J Clean Prod 2020. https://doi.org/10.1016/j.jclepro.2020.121231.

[49] Duan Z, Singh A, Xiao J, Hou S. Combined use of recycled powder and recycled coarse aggregate derived from construction and demolition waste in self-compacting concrete. Constr Build Mater 2020;254:119323. https://doi.org/10.1016/j.conbuildmat.2020.119323.
[50] Katkhuda H, Shatarat N. Improving the mechanical properties of recycled concrete aggregate using chopped basalt fibers and acid treatment. Constr Build Mater 2017;140:328–35. https://doi.org/10.1016/j.conbuildmat.2017.02.128.
[51] Alnahhal W, Aljidda O. Flexural behavior of basalt fiber reinforced concrete beams with recycled concrete coarse aggregates. Constr Build Mater 2018;169. https://doi.org/10.1016/j.conbuildmat.2018.02.135.
[52] Gao D, Zhang L. Flexural performance and evaluation method of steel fiber reinforced recycled coarse aggregate concrete. Constr Build Mater 2018;159:126–36. https://doi.org/10.1016/j.conbuildmat.2017.10.073.
[53] Mohseni E, Saadati R, Kordbacheh N, Parpinchi ZS, Tang W. Engineering and microstructural assessment of fibre-reinforced self-compacting concrete containing recycled coarse aggregate. J Clean Prod 2017;168:605–13. https://doi.org/10.1016/j.jclepro.2017.09.070.
[54] Dong JF, Wang QY, Guan ZW. Material properties of basalt fibre reinforced concrete made with recycled earthquake waste. Constr Build Mater 2017;130:241–51. https://doi.org/10.1016/j.conbuildmat.2016.08.118.
[55] Chen GM, He YH, Yang H, Chen JF, Guo YC. Compressive behavior of steel fiber reinforced recycled aggregate concrete after exposure to elevated temperatures. Constr Build Mater 2014;71:1–15. https://doi.org/10.1016/j.conbuildmat.2014.08.012.
[56] Taha A, Alnahhal W, Alnuaimi N. Bond durability of basalt FRP bars to fiber reinforced concrete in a saline environment. Compos Struct 2020;243:112277. https://doi.org/10.1016/j.compstruct.2020.112277.
[57] Al-Hamrani A, Alnahhal W. Shear behavior of basalt FRC beams reinforced with basalt FRP bars and glass FRP stirrups: experimental and analytical investigations. Eng Struct 2021;242:112612. https://doi.org/10.1016/j.engstruct.2021.112612.
[58] Zhang X, Shen Y, Fan Y, Gao X. Experimental study on the triaxial compression mechanical performance of basalt fiber-reinforced recycled aggregate concrete after exposure to high temperature. Case Stud Constr Mater 2024;20:e03026. https://doi.org/10.1016/J.CSCM.2024.E03026.
[59] Zhang X, Niu J, Qiao S, Luo C, Fan Y, Kuang X, et al. Study on eccentric compression mechanical characteristics of basalt fiber-reinforced recycled aggregate concrete-filled circular steel tubular column. 2023;13:1923 Coatings 2023;13:1923. https://doi.org/10.3390/COATINGS13111923.
[60] Zhang X, Niu J, Shen W, Deng D, Huang Y. Analysis of axial compression performance of BFRRAC-filled square steel tubular column. Steel Compos Struct 2023;49:457. https://doi.org/10.12989/SCS.2023.49.4.457.
[61] Hanafi M, Aydin E, Ekinci A. Engineering properties of basalt fiber-reinforced bottom ash cement paste composites. 2020;13:1952 Materials 2020;13:1952. https://doi.org/10.3390/MA13081952.
[62] Chen XF, Kou SC, Xing F. Mechanical and durable properties of chopped basalt fiber reinforced recycled aggregate concrete and the mathematical modeling. Constr Build Mater 2021;298:123901. https://doi.org/10.1016/J.CONBUILDMAT.2021.123901.
[63] Kim YJ, Choi YW. Utilization of waste concrete powder as a substitution material for cement. Constr Build Mater 2012;30:500–4. https://doi.org/10.1016/j.conbuildmat.2011.11.042.
[64] Ma Z, Liu M, Duan Z, Liang C, Wu H. Effects of active waste powder obtained from C&D waste on the microproperties and water permeability of concrete. J Clean Prod 2020;257:120518. https://doi.org/10.1016/j.jclepro.2020.120518.
[65] Wu H, Liu C, Zhao Y, Chen G, Gao J. Elucidating the role of recycled concrete powder in low-carbon ultra-high performance concrete (UHPC): multi-performance evaluation. Constr Build Mater 2024;441:137520. https://doi.org/10.1016/J.CONBUILDMAT.2024.137520.
[66] Vivek SS, Dhinakaran G. Fresh and hardened properties of binary blend high strength self compacting concrete. Eng Sci Technol, Int J 2017;20:1173–9. https://doi.org/10.1016/J.JESTCH.2017.05.003.
[67] Abushanab A, Alnahhal W. Performance of sustainable concrete incorporating treated domestic wastewater, RCA, and fly ash. Constr Build Mater 2022;329:127118. https://doi.org/10.1016/j.conbuildmat.2022.127118.
[68] ReforceTech - Reforcetech n.d. ⟨https://reforcetech.com/⟩ (accessed June 10, 2024).
[69] C192/C192M A. Standard practice for making and curing concrete test specimens in the laboratory. American Society for Testing and Materials 2014:1–8.
[70] ASTM C33/C33M - 18. Standard Specification for Concrete Aggregates. ASTM International 2018:1–8.
[71] ASTM C127-15. Standard test method for relative density (Specific Gravity) and absorption of coarse aggregate. ASTM 2015:1–5.
[72] ASTM C131 - 12. Standard test method for resistance to degradation of large -size coarse aggregate by abrasion and impact in the Los Angeles machine. ASTM International 2012:1–5. https://doi.org/10.1520/C0131.
[73] ASTM C. Standard test method for soundness of aggregates by use of sodium sulfate or magnesium sulfate. ASTM International 2013.
[74] ASTM C188-17. Standard test method for density of hydraulic cement. ASTM International 2017:1–3.
[75] ASTM C618-17a. Standard specification for coal fly ash and raw or calcined natural pozzolan for use in concrete. Annual Book of ASTM Standards 2017:1–5.
[76] ASTM C204. Standard test methods for fineness of hydraulic cement by air-permeability. ASTM International, West Conshohocken, PA 2018:1–10.
[77] ASTM C143/C143M. Standard test method for slump of hydraulic-cement concrete. ASTM C143 2015:1–4. https://doi.org/10.1520/C0143.
[78] ASTM C39/C39M. Standard test method for compressive strength of cylindrical concrete specimens. ASTM Standard Book 2021;i:1–5.
[79] ASTM C1609. Standard test method for flexural performance of fiber-reinforced concrete (using beam with third-point loading). ASTM International, West Conshohocken, PA 2012;i:9.
[80] AASHTO TP 95. Standard method of test for surface resistivity indication of concrete's ability to resist chloride ion penetration. American Association of State Highway and Transportation Officials, Washington, DC: 2011.
[81] ASTM C1202. Standard test method for electrical indication of concrete's ability to resist chloride ion penetration. American Society for Testing and Materials 2019:1–8.
[82] ASTMC642-21. C 642-21: Standard test method for density, absorption, and voids in hardened concrete. ASTM International 2021:11–3.
[83] ASTM C1723. Standard guide for examination of hardened concrete using scanning electron microscopy1. Annual Book of ASTM Standards 2016:1–9.
[84] Qatar General Organization for Standards and Metrology. Qatar construction specifications. 2014.
[85] Likes L, Markandeya A, Haider MM, Bollinger D, McCloy JS, Nassiri S. Recycled concrete and brick powders as supplements to Portland cement for more sustainable concrete. J Clean Prod 2022;364:132651. https://doi.org/10.1016/j.jclepro.2022.132651.
[86] Skripkiūnas G., Daukšys M., Štuopys A., Levinskas R. The influence of cement particles shape and concentration on the rheological properties of cement slurry. vol. 11. 2005.
[87] Shi D, Ye J, Zhang W. Effects of activator content on properties, mineralogy, hydration and microstructure of alkali-activated materials synthesized from calcium silicate slag and ground granulated blast furnace slag. J Build Eng 2020;32:101791. https://doi.org/10.1016/j.jobe.2020.101791.
[88] Jaya RP, Yusak MIM, Hainin MR, Mashros N, Warid MNM, Ali MI, et al. Physical and chemical properties of cement with nano black rice husk ash. AIP Conf Proc, 2151. American Institute of Physics Inc; 2019. https://doi.org/10.1063/1.5124654.
[89] Stutzman PE, Feng P, Bullard JW. Phase analysis of portland cement by combined quantitative X-ray powder diffraction and scanning electron microscopy. J Res Natl Inst Stand Technol 2016;121:47–107. https://doi.org/10.6028/jres.121.004.
[90] Fallahnejad H, Davoodi MR, Nikbin IM. The influence of aging on the fracture characteristics of recycled aggregate concrete through three methods. Struct Concr 2021;22:E74–93. https://doi.org/10.1002/suco.202000119.
[91] Poon CS, Shui ZH, Lam L. Effect of microstructure of ITZ on compressive strength of concrete prepared with recycled aggregates. Constr Build Mater 2004;18:461–8. https://doi.org/10.1016/j.conbuildmat.2004.03.005.
[92] Dimitriou G, Savva P, Petrou MF. Enhancing mechanical and durability properties of recycled aggregate concrete. Constr Build Mater 2018;158:228–35. https://doi.org/10.1016/j.conbuildmat.2017.09.137.
[93] Black L. Low clinker cement as a sustainable construction material. Sustainability of Construction Materials. Woodhead Publishing; 2016. p. 415–57. https://doi.org/10.1016/b978-0-08-100370-1.00017-2.
[94] Qureshi LA, Ali B, Ali A. Combined effects of supplementary cementitious materials (silica fume, GGBS, fly ash and rice husk ash) and steel fiber on the hardened properties of recycled aggregate concrete. Constr Build Mater 2020;263:120636. https://doi.org/10.1016/j.conbuildmat.2020.120636.
[95] Wu Z, Shi C, Khayat KH. Influence of silica fume content on microstructure development and bond to steel fiber in ultra-high strength cement-based materials (UHSC). Cem Concr Compos 2016;71:97–109. https://doi.org/10.1016/j.cemconcomp.2016.05.005.
[96] Ali B, Qureshi LA, Shah SHA, Rehman SU, Hussain I, Iqbal M. A step towards durable, ductile and sustainable concrete: simultaneous incorporation of recycled aggregates, glass fiber and fly ash. Constr Build Mater 2020;251:118980. https://doi.org/10.1016/j.conbuildmat.2020.118980.
[97] Thomas J, Thaickavil NN, Wilson PM. Strength and durability of concrete containing recycled concrete aggregates. J Build Eng 2018;19:349–65. https://doi.org/10.1016/j.jobe.2018.05.007.
[98] Lai M, Hanzic L, Ho JCM. Fillers to improve passing ability of concrete. Struct Concr 2019;20:185–97. https://doi.org/10.1002/suco.201800047.
[99] Dong S, Zhou D, Ashour A, Han B, Ou J. Flexural toughness and calculation model of super-fine stainless wire reinforced reactive powder concrete. Cem Concr Compos 2019;104:103367. https://doi.org/10.1016/j.cemconcomp.2019.103367.
[100] Khandelwal S, Rhee KY. Recent advances in basalt-fiber-reinforced composites: tailoring the fiber-matrix interface. Compos B Eng 2020;192:108011. https://doi.org/10.1016/j.compositesb.2020.108011.
[101] Shoaib S, El-Maaddawy T, El-Hassan H, El-Ariss B, Alsalami M. Fresh and hardened properties of concrete reinforced with basalt macro-fibers. Buildings 2022;12:1136. https://doi.org/10.3390/buildings12081136.
[102] Lai M, Hanzic L, Ho JCM. Fillers to improve passing ability of concrete. Struct Concr 2019;20:185–97. https://doi.org/10.1002/suco.201800047.
[103] Lee KM, Lee HK, Lee SH, Kim GY. Autogenous shrinkage of concrete containing granulated blast-furnace slag. Cem Concr Res 2006;36:1279–85. https://doi.org/10.1016/j.cemconres.2006.01.005.
[104] Seo J, Park S, Yoon HN, Lee HK. Effect of CaO incorporation on the microstructure and autogenous shrinkage of ternary blend Portland cement-slag-silica fume. Constr Build Mater 2020;249:118691. https://doi.org/10.1016/j.conbuildmat.2020.118691.
[105] Kaïkea A, Achoura D, Duplan F, Rizzuti L. Effect of mineral admixtures and steel fiber volume contents on the behavior of high performance fiber reinforced

concrete. Mater Des 2014;63:493–9. https://doi.org/10.1016/j.matdes.2014.06.066.
[106] Yodsudjai W, Nitichote K. Chloride penetration behavior of concrete made from various types of recycled concrete aggregate. Sustainability (Switzerland) 2022;14:2768. https://doi.org/10.3390/su14052768.
[107] Richardson DN. Strength and durability characteristics of a 70% ground granulated blast furnace slag (GGBFS). Concr Mix 2006;2006:94.
[108] Zhao H, Wang L, Wang D, Bai J, Fan Y. Effect of basalt fiber on chloride ion penetration of reactive powder concrete. IOP Conf Ser Mater Sci Eng 2020;711. https://doi.org/10.1088/1757-899X/711/1/012067.
[109] Tibbetts CM, Paris JM, Ferraro CC, Riding KA, Townsend TG. Relating water permeability to electrical resistivity and chloride penetrability of concrete containing different supplementary cementitious materials. Cem Concr Compos 2020;107:103491. https://doi.org/10.1016/j.cemconcomp.2019.103491.
[110] Sasanipour H, Aslani F. Durability properties evaluation of self-compacting concrete prepared with waste fine and coarse recycled concrete aggregates. Constr Build Mater 2020;236:117540. https://doi.org/10.1016/j.conbuildmat.2019.117540.
[111] Sengul O. Use of electrical resistivity as an indicator for durability. Constr Build Mater 2014;73:434–41. https://doi.org/10.1016/j.conbuildmat.2014.09.077.
[112] Lübeck A, Gastaldini ALG, Barin DS, Siqueira HC. Compressive strength and electrical properties of concrete with white Portland cement and blast-furnace slag. Cem Concr Compos 2012;34:392–9. https://doi.org/10.1016/j.cemconcomp.2011.11.017.
[113] Guo Y, Hu X, Lv J. Experimental study on the resistance of basalt fibre-reinforced concrete to chloride penetration. Constr Build Mater 2019;223:142–55. https://doi.org/10.1016/j.conbuildmat.2019.06.211.
[114] Jiang Y, Yan Y, Li T, Cao X, Yu L, Qi H. Comparison of the mechanical properties and crack expansion mechanism of different content and shapes of brass-coated steel fiber-reinforced ultra-high-performance concrete. Materials 2023;16:2257. https://doi.org/10.3390/ma16062257.
[115] Yuksel I. Blast-furnace slag. Waste and supplementary cementitious materials in concrete: characterisation, properties and applications. Woodhead Publishing; 2018. p. 361–415. https://doi.org/10.1016/B978-0-08-102156-9.00012-2.